Received February 19, 2015, accepted March 23, 2015, date of publication May 12, 2015, date of current version May 26, 2015.

Digital Object Identifier 10.1109/ACCESS.2015.2432015

Noncoherent Quantum Multiple Symbol Differential Detection for Wireless Systems

PANAGIOTIS BOTSINIS, (Student Member, IEEE), DIMITRIOS ALANIS, (Student Member, IEEE), ZUNAIRA BABAR, (Student Member, IEEE), SOON XIN NG, (Senior Member, IEEE), AND LAJOS HANZO, (Fellow, IEEE)

School of Electronics and Computer Science, University of Southampton, Southampton SO17 1BJ, U.K.

Corresponding author: L. Hanzo (lh@ecs.soton.ac.uk)

This work was supported in part by the India-U.K. Advanced Technology Centre, in part by the European Union through the Concerto Project and the European Research Council, in part by the Advanced Fellow Grant, and in part by Royal Society's Wolfson Research Merit Award.

ABSTRACT In large-dimensional wireless systems, such as cooperative multicell processing, millimeter-wave, and massive multiple input multiple output systems, or cells having a high user density, such as airports, train stations, and metropolitan areas, sufficiently accurate estimation of all the channel gains is required for performing coherent detection. Therefore, they may impose an excessive complexity. As an attractive design alternative, differential modulation relying on noncoherent detection may be invoked for eliminating the requirement for channel estimation at the base station, although at the cost of some performance degradation. In this treatise, we propose low-complexity hard-input hard-output, hard-input soft-output, as well as soft-input soft-output quantum-assisted multiple symbol differential detectors (MSDDs) that perform equivalently to the optimal, but highly complex maximum *a posteriori* probability MSDDs in multiuser systems, where the users are separated both in the frequency domain and in the time domain. When using an MSDD, the detection of a user's symbols is performed over windows of differentially modulated symbols; hence, they exhibit an increased complexity with respect to the conventional differential detector while simultaneously improving the performance of the system, especially at high Doppler frequencies.

INDEX TERMS Computational complexity, differential modulation, Dürr-Høyer algorithm, EXIT chart, Grover's quantum search algorithm, multiple input multiple output, multiple-symbol differential detection, non-coherent detection, orthogonal frequency division multiplexing, quantum computing.

LIST OF ABBREVIATIONS

AWGN	Additive White Gaussian Noise
BBHT	Boyer, Brassard, Høyer, Tapp
BER	Bit Error Ratio
CD	Classical Domain
CDD	Conventional Differential Detector
CF	Cost Function
CFE	Cost Function Evaluation
CoMP	Cooperative Multi-cell Processing
CSI	Channel State Information
DAPSK	Differential Amplitude and Phase Shift Keying
DEC	Decoder
DFDD	Decision-Feedback Differential Detectors
DHA	Dürr-Høyer Algorithm
DPSK	Differential Phase Shift Keying
DSS	Direct Sequence Spreading
EPA	Extended Pedestrian A
ES	Early-Stopping
EXIT	EXtrinsic Information Transfer
FBKT	Forward and Backward Knowledge Transfer
FKT	Forward Knowledge Transfer
HIHO	Hard-Input Hard-Output
HISO	Hard-Input Soft-Output
IFFT	Inverse Fast Fourier Transform
IpS	Iterations per Search
MAA	MAximum Approximation
MAP	Maximum *A posteriori* Probability
MBER	Minimum Bit Error Ratio
ML	Maximum Likelihood
MSDD	Multiple Symbol Differential Detector
MSDSD	Multiple Symbol Differential Sphere Detector
MUA	MUlti-input Approximation
MUD	Multi-User Detection
NE	Neighbour Exploitation

OFDM	Orthogonal Frequency Domain Multiplexing
PSAM	Pilot Symbol Assisted Modulation
QCA	Quantum Counting Algorithm
QCR	Quantum Control Register
QD	Quantum Domain
QMSDD	Quantum-assisted Multiple Symbol Differential Detection
QMUD	Quantum-assisted Multi-User Detection
QSA	Quantum Search Algorithm
QWSA	Quantum Weighted Sum Algorithm
SDMA	Spatial Division Multiple Access
SISO	Soft-Input Soft-Output
SNR	Signal to Noise Ratio
SSCH	Slow SubCarrier Hopping
Star-QAM	Star-Quadrature Amplitude Modulation
TC	Turbo Coding
USSCH	Uniform Slow SubCarrier Hopping

I. INTRODUCTION

When a fading channel's state experiences small fluctuations over several transmission periods, it is typically termed as a quasi-static channel, which hence only has to be estimated infrequently, hence imposing a moderate complexity. The channel estimation may be based on training by transmitting known pilot symbols to the receiver [1], [2]. Given the knowledge of the transmitted pilot symbol, the channel state may be estimated by comparing it to the noisy received pilot signal. In practice, the channel estimation does not offer perfect estimates of the channel states [3]–[5] due to a number of reasons, such as the limited number of pilots used, the dynamic nature of the channels and the noise. Semi-blind channel estimation [6], [7], which uses a reduced number of pilot signals, as well as totally blind channel estimation dispensing with pilots [8]–[10] may also be used for quasi-static channels.

When a fading channel's state changes rapidly between transmissions due to its high Doppler frequency, the density of pilot symbols in a Pilot Symbol Assisted Modulation (PSAM) frame [33] should be increased. When the density of the pilot symbols in a frame is increased, the effective throughput of the system is reduced. If the Doppler frequency of a fading channel is excessive, it may become infeasible to try and estimate the channel states, whilst simultaneously supporting an adequate throughput, since the density of pilot symbols required for performing accurate channel estimation will be too high.

Imperfect channel estimation in a multiple-access system results in a degradation of the performance of the Multi-User Detectors (MUD) [12], even though it gives a more realistic view of a practical system. In the emerging mm-Wave communication [34] and massive multiple input multiple output [3], [35]–[37] eras the number of transmit and receive antenna elements may be over 100 at each terminal, hence the total number of channels invoked in a single transmission may be over 10^4, essentially making the accurate estimation of their channel states impractical.

The family of non-coherent data detection schemes [3]–[5] relies on no channel estimation, for the sake of avoiding the computational complexity imposed by the channel estimation algorithms. Furthermore, since channel estimation is not required, apart from a reference symbol for each detection window, there is no need for pilot signals to be transmitted for this purpose, hence actually resulting in a higher system throughput and more efficient channel usage. On the other hand, the performance of a system relying on a non-coherent detector is worse than that of a system using a coherent detector as detailed in [3].

In the multiple access systems considered in this paper, the users' transmissions are orthogonal to each other in either the time domain, the frequency domain or the code domain and hence they may be readily separated without estimating their Channel State Information (CSI). Hence in this treatise we will focus our attention on differential modulation [3] and more specifically on Differential Phase Shift Keying (DPSK) [38]–[41]. In DPSK, the symbol transmitted in the tth time slot depends on the symbol transmitted during the $(t-1)$st time slot. It should be noted that multi-level differential modulation schemes, such as Differential Amplitude and Phase Shift Keying (DAPSK)/Star-Quadrature Amplitude Modulation (Star-QAM) [42]–[44], may also be employed for achieving higher throughput and frequency efficiency. At the receiver side, the non-coherent Conventional Differential Detector (CDD) [38]–[40] performs the inverse procedure and extracts the transmitted symbol based on the previously detected, differentially modulated symbol. The Multiple Symbol Differential Detector (MSDD) [38], [45], [46] makes a decision concerning all the most recent (N_w-1) differentially modulated and transmitted symbols, based on the most recent N_w received signals, where N_w is the decision window width. If we have $N_w = 2$, then the MSDD becomes equivalent to the CDD. It is expected that the higher the value of N_w, the more computationally demanding the MSDD becomes, but at the same time the BER performance of the system is improved. The classical Maximum Likelihood (ML) MSDD [3] is considered as the optimal but high-complexity non-coherent Hard-Input Hard-Output (HIHO) MSDD. Both the Decision-Feedback Differential Detector (DFDD) [39], [47]–[49] and the Multiple Symbol Differential Sphere Detector (MSDSD) [50]–[52] are attractive non-coherent detectors, since they offer a near-optimal performance with respect to the MSDD whilst imposing a reduced complexity. The Soft-Input Soft-Output (SISO) versions of the MSDD [45], namely the DFDD [53]–[55] and the MSDSD [56] may be integrated into an iterative receiver, where extrinsic information is exchanged between the channel decoders and the multiple symbol detectors as detailed in [3]. In a severe multipath fading environment, both the coherent and non-coherent data detection schemes experience a degraded performance [3]. However, fast fading

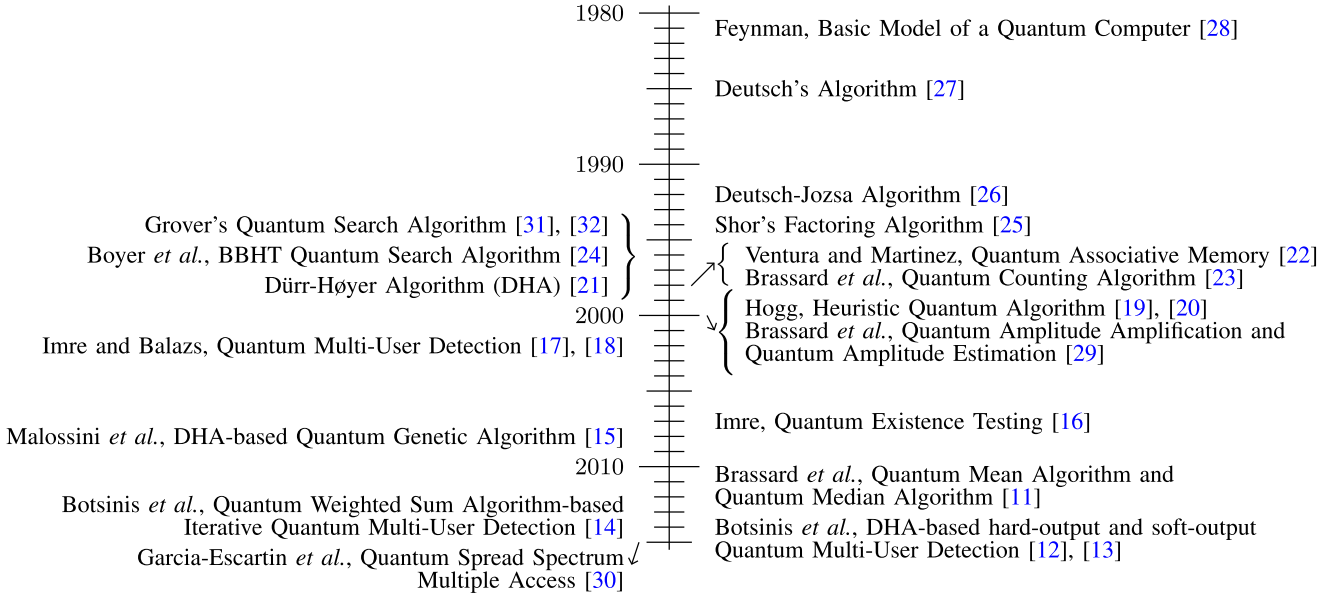

FIGURE 1. **Selected contributions in the field of quantum search algorithms and applications of quantum computing in wireless systems.**

has a more catastrophic impact on differentially encoded systems with non-coherent signal detection, due to the assumption engraved in the methodology of such systems that the channel coefficients of two consecutive symbols are identical [3].

The optimization procedures invoked by the MSDDs for finding the most likely decision candidate for the transmitted multi-level symbols may be successfully implemented at the cost of a reduced number of Cost Function Evaluations (CFE) with the aid of quantum computing [57]–[59]. More specifically, Grover's Quantum Search Algorithm (QSA) [31], [32] may be invoked, which successfully solves a specific search problem by finding a specific entry in a database of N candidates by requiring as few as $O(\sqrt{N})$ queries, while classically we have to perform $O(N)$ queries. The more advanced Dürr-Høyer Algorithm (DHA) [21] finds the particular index that corresponds to the minimum entry in an N-element database by also requiring as few as $O(\sqrt{N})$ queries, while the optimal classical algorithm needs N queries. Fig. 1 summarizes the main contributions in quantum search algorithms, including their applications in the detection problems of wireless systems.

In the context of multiple-stream detection in wireless communications, in their seminal paper Imre and Balazs proposed a low-complexity HIHO Quantum-assisted MUD (QMUD) [17] based on the Quantum Counting Algorithm (QCA) [23], [24]. Furthermore, we have also proposed a number of QMUDs [12]–[14], [60], which achieve a HIHO and a SISO performance equivalent to those of the ML MUD and of the Maximum *A posteriori* Probability (MAP) MUD, respectively, while imposing a substantially reduced number of CFEs, especially in high-dimensional rank-deficient systems having more transmitters than receivers, hence exhibiting a non-invertible channel matrix. All the aforementioned detectors require the accurate knowledge of all the CSIs. The complexity of the related multiple-stream detectors may be quantified in terms of the number of database queries or CFEs performed [12], [14], [24], [31].

Based on the current state-of-the-art, our novel contributions are:

1) *We propose attractive low-complexity HIHO, Hard-Input Soft-Output (HISO) and SISO Quantum-assisted MSDDs, which require no knowledge of the CSI, hence eliminating the computational complexity that would be required by the channel estimation procedure for providing accurate channel estimates. More specifically,*
   - *We conceive both the SISO DHA-aided QMSDD relying on MUlti-input Approximation (MUA) and the DHA-aided Quantum Weighted Sum Algorithm (QWSA) assisted QMSDD, both of which achieve a performance equivalent to that of the MAP MSDD, while requiring a substantially lower number of CFEs than the MAP MSDD.*
   - *We design the DHA-aided MAximum Approximation (MAA) QMSDD, which may be used for non-iterative soft-output data detection and has a lower number of CFEs sthan the DHA-MUA QMSDD and the DHA-QWSA QMSDD.*
   - *We propose the HIHO DHA-based and Early-Stopping-aided (ES) DHA QMSDD, followed by comparing their performances to that of the optimal HIHO ML MSDD.*
2) *The QMSDDs are employed in multi-user Direct Sequence Spreading (DSS) and Slow SubCarrier Hopping (SSCH)-aided Spatial Division Multiple Access (SDMA) systems intrinsically amalgamated*

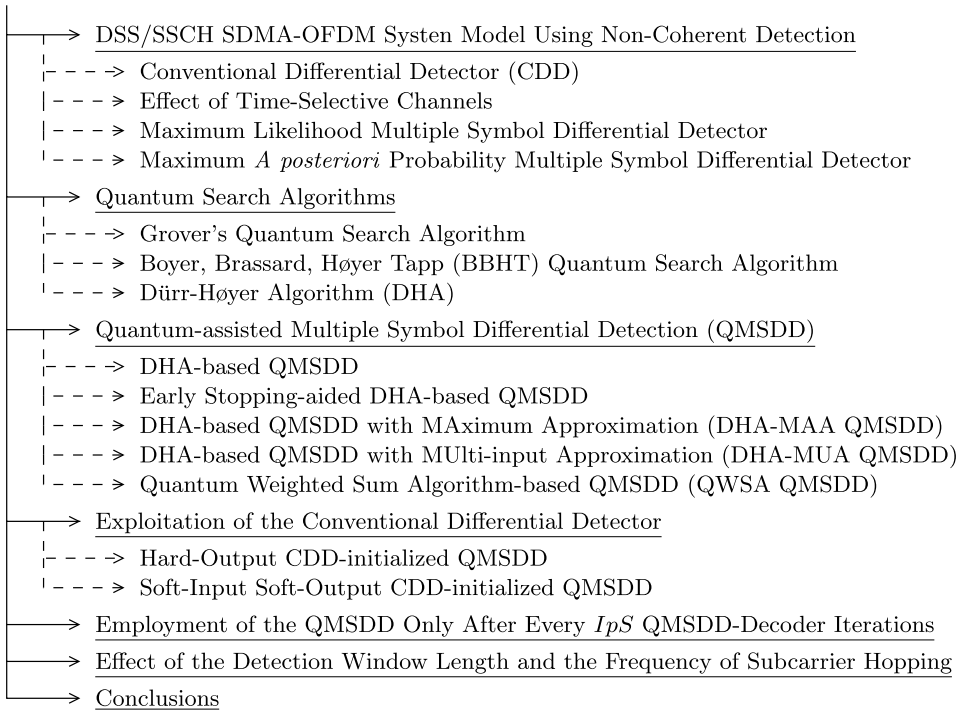

FIGURE 2. Summary of the sections of the paper.

with Orthogonal Frequency Domain Multiplexing (OFDM), where the users are separated in the frequency, time or code domain. The QMSDDs' performance is evaluated based on their Bit Error Ratio (BER) versus E_b/N_0 plots, as well as on EXtrinsic Information Transfer (EXIT) charts.

3) *A novel methodology is designed for deterministically initializing the DHA for the proposed QMSDDs for the sake of reducing the receiver's complexity by exploiting the CDD.*
4) *For further lowering the detector's complexity invoked in our iterative receivers, the SISO QMSDDs are not activated during every single MSDD - DECoder (DEC) iteration, whilst mitigating the resultant performance degradation.*
5) *The effect of the detection window length N_w employed in the QMSDDs, that of the interleaver length and of the SSCH period on the QMSDDs' performance is investigated.*

The rest of the paper is structured as depicted in Fig. 2. In Section II we analyse the DPSK modulation scheme, the ML MSDD and the MAP MSDD in the context of a DSS/SSCH SDMA-OFDM system. In Section III we present the quantum search algorithms, as well as the necessary quantum computing background, while in Section IV we propose the HIHO, HISO and SISO QMSDDs. Furthermore, we exploit the CDD for deterministically initializing the QMSDD in Section V and employ the QMSDD every *IpS* number of QMSDD-DEC iterations in Section VI. Section VII investigates the effect that the detection window length and the SSCH period have on the system's performance. Finally, our conclusions are offered in Section VIII.

II. DSS/SSCH SDMA-OFDM SYSTEM MODEL USING NON-COHERENT DETECTION

The DSS/SSCH SDMA-OFDM system model relying on non-coherent detection [3] is presented in Fig. 3. The system supports U users, each of whom encodes his / her information bits $\{b_u\}$, $u \in \{1, 2, \ldots, U\}$, using a turbo convolutional encoder, resulting in the encoded bit sequence $\{c_u\}$.

After the encoded bit sequence has been interleaved, the bit sequence $\{d_u\}$ is separated into W parallel streams, where W is the number of subcarriers associated to each user. Let us assume that Q subcarriers are available in our system and that the length of each user's symbol stream is equal to Γ symbols. Therefore, we have $W \leq Q$, $W \leq \Gamma$ and $\mod(\Gamma, W) = 0$. It should be noted at this stage that the user-specific scheduling of the subcarrier allocation algorithm is assumed to change every T_h OFDM symbol periods. The subcarrier allocation procedure follows the DSS-aided Uniform SSCH (USSCH) [13] algorithm performed at the BS.

Each parallel stream is differentially encoded by the DMPSK Symbol Mapping block of Fig. 3. Let us assume that conventional M-ary PSK modulation having a mapping set $\mathcal{M} = \{2\pi m/M;\ m = 0, 1, \ldots M-1\}$ is chosen. Furthermore, we omit the user subscript without any loss of generality, since the same procedure occurs at each user's terminal. The first transmitted symbol $s[0]$ is termed as the reference symbol, which is assumed to be known

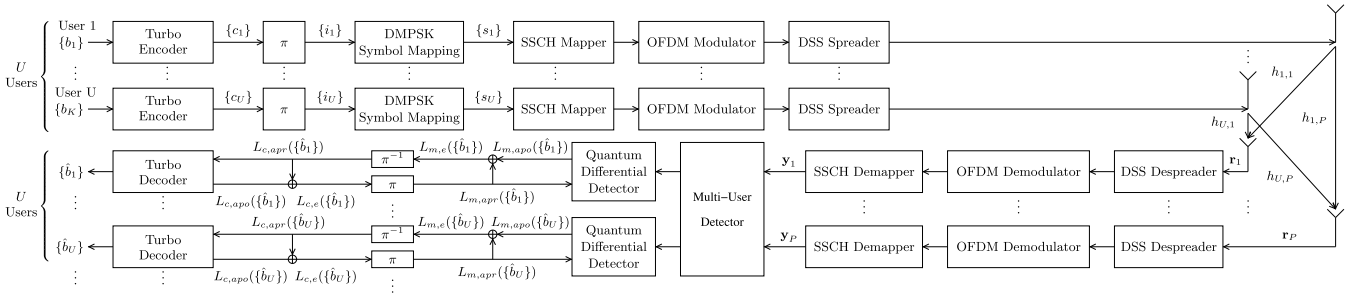

FIGURE 3. System model of a direct-sequence and slow subcarrier-hopping aided SDMA-OFDM system with differential modulation and a receiver with non-coherent MSDD.

at the receiver. After $\log_2(M_c)$ bits have been mapped to an M_c-ary PSK symbol $x[t]$ during the tth time slot, the resultant symbol is multiplied by the symbol transmitted during the $(t-1)$st time slot $s[t-1]$, as encapsulated in

$$s[t] = s[t-1] \cdot x[t]. \tag{1}$$

Then, $s[t]$ is buffered at the transmitter for encoding $s[t+1]$, following (1).

Each of the W differentially encoded symbol sequences $\{s_{u,w}\}$ of the uth user are then mapped to the respective subcarriers based on the schedule received by the BS. The differential detection carried out at the receiver is based on the assumption that the multipath Rayleigh channel states change very slowly in that specific domain where the differential encoding took place. In this treatise we have opted for the differential encoding to take place in the time domain, hence the channels are assumed to experience slow fading. Since the subcarrier allocation schedule changes every T_h OFDM symbol periods for each user, it is not reasonable to assume that the channel state of the uth user on the qth subcarrier will be similar to that of the same user on the jth subcarrier after a new subcarrier allocation schedule associated with $j \neq q$. Therefore, the differential encoding procedure of the DMPSK symbol mapping block seen in Fig. 3 occurs in blocks of T_h symbols on each of the W parallel streams of the uth user. This architecture ensures that a new reference symbol is transmitted every time the subcarriers the uth user transmits on are changed. A visual representation of N_w and T_h is depicted in Fig. 4. It is logical to expect that when T_h is increased, the channel-correlation between the differentially encoded symbols is also increased. Therefore, if an MSDD is used in conjunction with $N_w = T_h$, the performance will be improved. However, at the same time, the complexity of the MSDD becomes higher. Furthermore, in the same scenario, the users who have been allocated gravely faded subcarriers suffer from prolonged frames, since the channel states vary slowly.

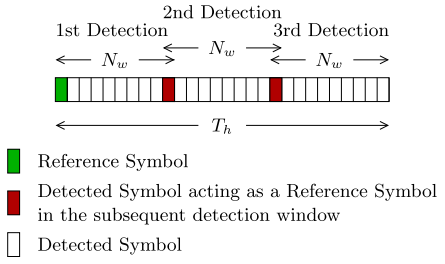

FIGURE 4. Visual representation of T_h and N_w for the uth user on the qth subcarrier.

Following the SSCH mapper of Fig. 3, the OFDM modulator modulates the symbols of each user by performing a Q-point Inverse Fast Fourier Transform (IFFT). The symbols are then spread in the time domain by a DSS spreader, using a user-specific spreading sequence associated with a spreading factor of SF. Let us use $G = SF$-chip Walsh-Hadamard spreading codes, which are orthogonal to each other. The allocation of the G number of WH spreading codes to the U users may be performed as in

$$\left\lfloor \frac{U}{G} \right\rfloor + \begin{cases} 1 & \text{if } g < \text{mod}(U, G) \\ 0 & \text{if } g \geq \text{mod}(U, G), \end{cases} \tag{2}$$

where $g \in \{1, 2, \ldots, G\}$. Following the DSS spreading scheme in Fig. 3 in the time domain, the symbols are transmitted over multipath Rayleigh channels to the BS.

In this treatise the systems we investigate have users supported by the same DSS code allocated to different subcarriers. Therefore, there is no need to perform non-coherent multi-user detection in the spatial domain, since there will be no users who interfere with each other, because we use orthogonal WH codes. These scenarios assist us in focusing our attention on non-coherent MSDD, rather than on non-coherent MUD.

Still considering Fig. 3, after the signals of the U users have been transmitted, they are received by the P receive AEs at the BS. Naturally, the users who transmit on different subcarriers do not interfere with each other, since they are separated in the frequency domain. In this treatise we assume the employment of a synchronous system, therefore all the received signals are synchronously superimposed at the pth receive AE, with $p \in \{1, 2, \ldots, P\}$. Furthermore, Additive White Gaussian Noise (AWGN) is added at each receive AE, having a zero mean and a variance of $N_0 = 2\sigma^2$. The DSS despreader of Fig. 3 then despreads the signals received on each receive AE in the time domain. At this

stage, the users who transmit on the same subcarrier and have been allocated different orthogonal DSS codes are separated. Afterwards, the received OFDM symbol is demodulated on the pth receive AE chain by using the Q-point FFT. Finally, the demodulated symbols transmitted on different subcarriers are dehopped and fed to the MUD / Differential Detector.

For the analysis of differential detectors, let us focus our attention on the signal processing of the qth subcarrier and the pth receive AE chain. Let us assume that $U_{g,q}$ users have been allocated the gth DSS code on the qth subcarrier, U_q users transmit on the qth subcarrier, with $1 \leq U_q \leq U$, while G_q different DSS codes are present on the qth subcarrier, with $1 \leq G_q \leq G$. Since in our differential detection scenarios we allow at most one user belonging to a single DSS group to transmit on the qth subcarrier, we have $U_q = G_q$ and $U_{q,g} = 1$. Therefore, the signal $\mathbf{r}_{p,q}$ received in our synchronous DSS/SSCH SDMA-OFDM system on the qth subcarrier at the pth receive AE is expressed as [3]

$$\mathbf{r}_{p,q} = \bar{\mathbf{c}}_{G_q} \bar{\mathbf{H}}_{p,q} \bar{\mathbf{s}}_q + \mathbf{n}_{p,q}, \tag{3}$$

where $\bar{\mathbf{c}}_{G_q}$ is the $(SF \times U_q) = (SF \times G_q)$-element matrix that contains the DSS codes of the U_q users on the qth subcarrier, as in [3]

$$\bar{\mathbf{c}}_{G_q} = [\underbrace{\mathbf{c}_1, \ldots, \mathbf{c}_1}_{U_{q,1}=1}, \underbrace{\mathbf{c}_2, \ldots, \mathbf{c}_2}_{U_{q,2}=1}, \ldots, \underbrace{\mathbf{c}_{G_q}, \ldots, \mathbf{c}_{G_q}}_{U_{q,G_q}=1}] \tag{4}$$

$$= [\mathbf{c}_1, \mathbf{c}_2, \ldots, \mathbf{c}_{G_q}], \tag{5}$$

where $\mathbf{c}_g$ is the gth DSS code, represented by a $(SF \times 1)$-element vector as in

$$\mathbf{c}_g = \left[c_g[1], c_g[2], \ldots, c_g[SF] \right]^T, \tag{6}$$

and $c_g[i]$ is the value of the ith chip of the gth DSS code, with $g \in \{1, 2, \ldots, G_q\}$ and $c_g[i] \in \{-\frac{1}{\sqrt{SF}}, +\frac{1}{\sqrt{SF}}\}$. Furthermore, the $\bar{\mathbf{H}}_{p,q}$ matrix in (3) represents the $(U_q \times U_q)$-element FD-CHTF matrix of the channel states on the qth subcarrier between the U_q users and the pth receive AE, which is represented as [3]

$$\bar{\mathbf{H}}_{p,q} = \text{diag}\left[h^{(1)}_{p,1,q}, h^{(1)}_{p,2,q}, \ldots, h^{(1)}_{p,G_q,q} \right] \tag{7}$$

$$= \text{diag}\left[h_{p,1,q}, h_{p,2,q}, \ldots, h_{p,G_q,q} \right], \tag{8}$$

where $h^{(i)}_{p,g,q}$ is the complex-valued channel state in the frequency domain on the qth subcarrier between the ith user in the gth DSS code group and the pth receive AE, where the fact that we have $U_{q,g_q} = 1$ was exploited, with $g_q \in \{1, 2, \ldots, G_q\}$. Since in our non-coherent scenarios we have allowed only one user, if any, from a single DSS code group to be mapped to a subcarrier, we have $i = 1$ if the gth DSS code is present on the qth subcarrier. Therefore, we may omit the superscript (i) corresponding to the user index in the gth DSS code group. Moreover, the $(U_q \times 1)$-element symbol vector $\bar{\mathbf{s}}_q$ in (3) represents the differentially encoded symbols of the U_q users who transmit on the qth subcarrier, as in [3]

$$\bar{\mathbf{s}}_q = \left[s^{(1)}_{1,q}, s^{(1)}_{2,q}, \ldots, s^{(1)}_{G_q,q} \right]^T \tag{9}$$

$$= \left[s_{1,q}, s_{2,q}, \ldots, s_{G_q,q} \right]^T, \tag{10}$$

where $s^{(i)}_{g,q}$ is the differentially encoded symbol transmitted by the ith user of the gth DSS group on the qth subcarrier. Once again, in our system we have $i \in \{0, 1\}$, therefore we may omit the superscript (i) as we did in (10). Finally, the $(1 \times SF)$-element noise vector $n_{p,q}$ with zero mean and a variance equal to $N_0 = 2\sigma^2$ is represented as [3]

$$\mathbf{n}_{p,q} = \left[n_{p,q}[1], n_{p,q}[2], \ldots, n_{p,q}[SF] \right]^T. \tag{11}$$

After the DSS despreading procedure, the $(G_q \times 1)$-element symbol vector mapped to the qth subcarrier at the pth receive AE chain $\bar{\mathbf{y}}_{p,q}$ is equal to [3]

$$\bar{\mathbf{y}}_{p,q} = \check{\mathbf{c}}_{G_q} \mathbf{r}_{p,q} \tag{12}$$

$$= \bar{\mathbf{R}}_{G_q} \bar{\mathbf{H}}_{p,q} \bar{\mathbf{s}}_q + \bar{\mathbf{n}}_{p,q}, \tag{13}$$

where $\check{\mathbf{c}}_{G_q}$ is the $(SF \times G_q)$-element code book, containing all the different DSS codes that appear on the qth subcarrier, as in [3]

$$\check{\mathbf{c}}_{G_q} = \left[\mathbf{c}_1, \mathbf{c}_2, \ldots, \mathbf{c}_{G_q} \right]^T, \tag{14}$$

where $\mathbf{c}_g$ is the DSS code presented in (6). In our system, where a maximum of one user of the gth DSS code group is allowed to transmit on the qth subcarrier, we have

$$\check{\mathbf{c}}_{G_q} = \left(\bar{\mathbf{c}}_{G_q} \right)^T, \tag{15}$$

where $\bar{\mathbf{c}}_{G_q}$ is given in (5). In (13), the $(G_q \times 1)$-element noise vector $\bar{\mathbf{n}}_{p,q}$ represents the effective noise and is given in

$$\bar{\mathbf{n}} = \check{\mathbf{c}}_{G_q} \mathbf{n}_{p,q} \tag{16}$$

$$= \left[n_{p,1,q}, n_{p,2,q}, \ldots, n_{p,G_q,q} \right]^T. \tag{17}$$

Finally, $\bar{\mathbf{R}}_{G_q}$ in (13) is the $(SF \times U_q)$-element cross-correlation matrix of the G_q DSS codes that are present on the qth subcarrier, as formulated in

$$\bar{\mathbf{R}}_{G_q} = \begin{bmatrix} \omega_{11} & \omega_{12} & \cdots & \omega_{1G_q} \\ \omega_{21} & \omega_{22} & \cdots & \omega_{2G_q} \\ \vdots & \vdots & \ddots & \vdots \\ \omega_{G_q1} & \omega_{G_q2} & \cdots & \omega_{G_qG_q} \end{bmatrix}, \tag{18}$$

where $\omega_{i,j}$ is the cross-correlation between the ith and the jth DSS code, where $U_{q,i} = 1$ was exploited. Since we have chosen orthogonal WH codes in our system, the cross-correlation matrix in (18) is equal to the identity matrix, because we have:

$$\omega_{i,j} = \begin{cases} 1 & \text{if } i = j \\ 0 & \text{if } i \neq j. \end{cases} \tag{19}$$

In the end, the signal $\bar{\mathbf{y}}_{p,q}$ in (13) becomes

$$\bar{\mathbf{y}}_{p,q} = \bar{\mathbf{R}}_{G_q} \bar{\mathbf{H}}_{p,q} \bar{\mathbf{s}}_q + \bar{\mathbf{n}}_{p,q}. \tag{20}$$

In the following sections the same differential detection process will be applied for every user's symbol stream, having been allocated a DSS code and transmitting on their allocated subcarriers, therefore we may omit the u, g and q subscripts without any loss of generality.

A. CONVENTIONAL DIFFERENTIAL DETECTOR

The signals received during the $(t-1)$st and tth time slots at the pth receive AE are

$$y_p[t-1] = h_p[t-1] \cdot s[t-1] + n_p[t-1] \quad (21)$$

$$y_p[t] = h_p[t] \cdot s[t] + n_p[t], \quad (22)$$

respectively, where $h_p[t-1]$ and $h_p[t]$ denote the channel states at the $(t-1)$st and tth time slots, respectively, between the user and the pth receive AE, while $n_p[t-1]$ and $n_p[t]$ are the AWGN samples imposed on the pth receive AE at the $(t-1)$st and tth time slots, respectively. Each of the noise samples $n_p[t-1]$ and $n_p[t]$ have zero mean and a variance of $2\sigma^2$. Assuming that the transmissions occur over slow-fading channels, we have

$$h_p[t-1] = h_p[t], \quad \forall p = 1, 2, \ldots, P \quad (23)$$

for every time slot that corresponds to the same transmitted frame after the most recent reference symbol was transmitted. It should be noted that (23) represents the main assumption of non-coherent detection, but it does not imply that $h_p[t-1] = h_p[t]$ is necessarily true in the actual channel. Therefore, the more the channel varies in time, the more inaccurate the assumption in (23) becomes, and hence the worse the performance of the non-coherent detector is expected to be. By substituting (23) into (21) and (22), we arrive at:

$$y_p[t] = h_p[t-1] \cdot s[t-1] \cdot x[t] + n_p[t] \quad (24)$$

$$= y_p[t-1] \cdot x[t] + \underbrace{n_p[t] - n_p[t-1] \cdot x[t]}_{n'_p[t]}. \quad (25)$$

Therefore, the M-ary symbol $x[t]$ may be obtained by following the same procedure as in a single-input multiple-output channel, where $y_p[t-1]$ is the reference signal, or the "known" channel state, and $n'_p[t]$ is the effective noise with a variance of $4\sigma^2$, since $n_p[t]$ and $n_p[t-1]$ are added. The resultant decision concerning $x[t]$ is performed as in

$$x[t] = \arg\min_{x \in \mathcal{M}} \left(\left| x - \sum_{p=1}^{P} \frac{y_p[t]}{y_p[t-1]} \right|^2 \right), \quad (26)$$

where $y_p[t-1]$ and $y_p[t]$ are described in (21) and (22), respectively. The advantage of detecting the desired symbol without requiring an estimate of the channel state is gleaned at the cost of a 3 dB penalty due to the noise [3]. Even though a higher transmission power is required in non-coherent systems for achieving the same performance as their coherent counterparts, the complexity of the non-coherent receivers is typically much lower.

It should be noted that we employ a practical system, where we experience continuous Rayleigh fading at the subcarriers. Therefore, if the normalized Doppler frequency of the independent Rayleigh channels on each tap of the multipath channel model is equal to f_d and we have Q subcarriers, the effective Doppler frequency between the channel states of two consecutively received symbols on the qth subcarrier is equal to

$$F_d = f_d \cdot Q. \quad (27)$$

In other words, the effective channel that a subcarrier experiences in the time domain has a Doppler frequency of F_d given by (27).

B. EFFECT OF TIME-SELECTIVE CHANNELS

The DPSK modulation may be performed for the consecutive symbols in the time domain, for consecutive OFDM symbols of the same subcarriers. It may also be carried out in the frequency domain, by differentially encoding the symbols of the adjacent subcarriers of the same OFDM symbol. In this treatise, we will proceed by applying differential modulation in the time domain. Therefore, according to the slow-fading assumption made in (23) about the channels, time-selective channels are expected to impose a major effect on the differential detection in our systems. This is characterized by the autocorrelation function of the channel states between the uth user and the pth receive AE on the qth subcarrier, which is [3]

$$\phi^t_{hh}[\kappa] \triangleq \mathcal{E}\left\{ h_p[t+\kappa] \cdot h^*_p[t] \right\} = J_0\left(2\pi F_d \kappa\right), \quad (28)$$

where $J_0(\cdot)$ is the zeroth-order Bessel function, f_d is the normalized Doppler frequency of the channels, while F_d is the effective normalized Doppler frequency of the channels as described in (27).

C. MAXIMUM LIKELIHOOD MULTIPLE SYMBOL DIFFERENTIAL DETECTOR [3]

The performance of the CDD mainly depends on the accuracy of the detection, since every decision made for the most recently received symbol affects the detection of the next symbol. The MSDD performs detection on N_w consecutively received symbols with $N_w > 2$. The BER performance of the MSDDs is assumed to be better than that of the CDD, since the correlation between the phase distortions of symbols that were transmitted with more than one symbol period difference is also taken into consideration in the detection. On the other hand, the complexity of any MSDD is higher than that of the CDD, since the problem becomes a "shortest-vector" problem [3] and the pool of legitimate candidates increases exponentially with N_w. Since the reference symbol is known to the receiver, the MSDD performing detection over N_w received symbols determines the estimates of $(N_w - 1)$ symbols.

As in the CDD section, the following analysis takes place at the differential detection stage of Fig. 3. We focus

our attention on the uth user, having been assigned the gth DSS code and transmitting on the qth subcarrier, therefore we omit the subscripts u, g and q. Furthermore, the symbols described in (20) are assumed to be available. The number of OFDM symbols transmitted between two reference symbols is equal to T_h.

Since the detection is performed in blocks of N_w symbols, with the consecutive blocks overlapping by one symbol, the ith received symbol vector, $i \in \{1, 2, \ldots, T_h/N_w\}$, at the pth receive AE consisting of N_w consecutively received symbols in the time domain is

$$\mathbf{y}_p[i] \triangleq [y_p[N_w \cdot i - (N_w - 1)],\ y_p[N_w \cdot i - (N_w - 2)], \ldots, y_p[N_w \cdot i]]^T. \quad (29)$$

The received symbol vector of (29) is exploited by the MSDD for estimating the ith N_w-element transmitted symbol vector $\hat{\mathbf{s}}[i]$, which corresponds to the ith actually transmitted symbol vector

$$\mathbf{s}[i] \triangleq [s[N_w \cdot i - (N_w - 1)],\ s[N_w \cdot i - (N_w - 2)], \ldots,\ s[N_w \cdot i]]^T, \quad (30)$$

which in turn is the differentially encoded version of the $(N_w - 1)$-element symbol vector

$$\mathbf{x}[i] \triangleq [x[N_w \cdot i - (N_w - 2)],\ x[N_w \cdot i - (N_w - 3)], \ldots,\ x[N_w \cdot i]]^T. \quad (31)$$

The objective of the MSDD is to find the best estimate $\hat{\mathbf{x}}[i]$ of the symbol vector in (31). The MSDD performs detection on a block-by-block basis, therefore we may omit the subscript i in (29), (30) and (31) from our analysis, resulting in

$$\mathbf{y}_p \triangleq [\, y_p[1],\ y_p[2],\ \ldots\ ,\ y_p[N_w]\,]^T, \quad (32)$$
$$\mathbf{s} \triangleq [\, s[1],\ s[2],\ \ldots\ ,\ s[N_w]\,]^T, \quad (33)$$
$$\mathbf{x} \triangleq [\, x[2],\ x[3],\ \ldots\ ,\ x[N_w]\,]^T. \quad (34)$$

The conditional PDF of the received symbol vector $\mathbf{y}$ of (32) over N_w consecutive OFDM symbols, given that the symbol vector $\mathbf{s}$ of (33) was transmitted, is [50]

$$p(\mathbf{Y}|\mathbf{s}) = \frac{\exp\left(-Tr\left\{\mathbf{Y}^H \Psi^{-1} \mathbf{Y}\right\}\right)}{\left(\det\{\pi \Psi\}\right)^P}, \quad (35)$$

where $\mathbf{Y}$ is the $(N_w \times P)$-element matrix that contains the P number of received symbol vectors $\mathbf{y}_p$, $p \in \{1, 2, \ldots, P\}$, as in

$$\mathbf{Y} = [\mathbf{y}_1, \mathbf{y}_2, \ldots, \mathbf{y}_P] \quad (36)$$

and $Tr\{\cdot\}$ yields the trace of a square matrix. Furthermore, $\Psi = \mathcal{E}\left\{\mathbf{y}_p \mathbf{y}_p^H | \mathbf{s}\right\}$ is the $(N_w \times N_w)$-element conditional autocorrelation matrix of the Rayleigh channel. The conditional autocorrelation matrix of the Rayleigh channel Ψ in (35) depends on the transmitted symbol vector $\mathbf{s}$, the noise variance N_0 and the normalized Doppler frequency F_d, therefore it is the same for each of the P receive AEs, hence allowing us to omit the subscript p from the following discussion of Ψ. It may be expanded as

$$\Psi = \mathcal{E}\left\{\mathbf{y}\mathbf{y}^H | \mathbf{s}\right\} \quad (37)$$
$$= \mathrm{diag}(\mathbf{s}) \cdot \mathcal{E}\left\{\mathbf{h}\mathbf{h}^H\right\} \cdot \mathrm{diag}(\mathbf{s}^H) + \mathcal{E}\left\{\mathbf{n}\mathbf{n}^H\right\} \quad (38)$$
$$= \mathrm{diag}(\mathbf{s}) \cdot \left(\mathcal{E}\left\{\mathbf{h}\mathbf{h}^H\right\} + 2\sigma^2 \cdot \mathbf{I}_{N_w}\right) \cdot \mathrm{diag}(\mathbf{s}^H) \quad (39)$$
$$= \mathrm{diag}(\mathbf{s}) \cdot \mathbf{C} \cdot \mathrm{diag}(\mathbf{s}^H), \quad (40)$$

where $\mathbf{C} \triangleq \mathcal{E}\left\{\mathbf{h}\mathbf{h}^H\right\} + 2\sigma^2 \cdot \mathbf{I}_{N_w}$ and $\mathrm{diag}(\mathbf{s})$ is a diagonal matrix with the vector $\mathbf{s}$ on its diagonal. Since we have chosen to differentially encode the symbols in the time domain, Σ_h may be represented as

$$\Sigma_h = \mathcal{E}\left\{\mathbf{h}\mathbf{h}^H\right\} \quad (41)$$
$$= \sigma_h^2 \cdot \begin{bmatrix} \phi_{hh}^t[0] & \phi_{hh}^t[1] & \cdots & \phi_{hh}^t[N_w - 1] \\ \phi_{hh}^t[1] & \phi_{hh}^t[0] & \cdots & \phi_{hh}^t[N_w - 2] \\ \vdots & \vdots & \ddots & \vdots \\ \phi_{hh}^t[N_w - 1] & \phi_{hh}^t[N_w - 2] & \cdots & \phi_{hh}^t[0] \end{bmatrix},$$

where σ_h^2 is the variance of the channel and $\phi_{hh}^t[\kappa]$, $k \in \{0, 1, \ldots, N_w - 1\}$, is the autocorrelation function of the channel states in the time domain, which is stated in (28).

In non-coherent receivers, where no channel coding has been applied, the performance of HIHO MSDDs will be equivalent to the performance of SISO MSDDs, provided that the legitimate symbols are transmitted with equal probability, but the required complexity is smaller. In HIHO MSDDs, the detection is performed by finding that particular multi-level symbol estimate $\hat{\mathbf{x}}$ of (34), or, equivalently, $\hat{\mathbf{s}}$ of (33), which minimizes a specific metric, thus transforming the problem into a "shortest-vector" problem [50]. More specifically, the ML MSDD detects that particular symbol vector $\hat{\mathbf{s}}$, which maximizes the probability of $\hat{\mathbf{s}}$ having been transmitted, given that the symbol matrix $\mathbf{Y}$ has been received, or, in other words

$$\hat{\mathbf{s}}_{ML} = \arg\max_{\mathbf{s} \in \mathcal{M}^{N_w}} (P(\mathbf{s}|\mathbf{Y})) = \arg\max_{\mathbf{s} \in \mathcal{M}^{N_w}} \left(\frac{p(\mathbf{Y}|\mathbf{s}) \cdot P(\mathbf{s})}{p(\mathbf{Y})}\right) \quad (42)$$

where the Bayes' theorem [61], [62] was applied. Still referring to (42), $p(\mathbf{Y}|\mathbf{s})$ is the conditional probability of having received the symbol matrix $\mathbf{Y}$, given that $\mathbf{s}$ was transmitted as in (35), $P(\mathbf{s})$ is the *a priori* probability of the symbol vector $\mathbf{s}$ to have been transmitted and $p(\mathbf{Y})$ is termed as the system model probability, which represents the probability of having received $\mathbf{Y}$. Considering that a HIHO receiver is non-iterative and that the transmitter generated the source bits equiprobably, the values of $p(\mathbf{Y})$ and $P(\mathbf{s})$ are the same for every legitimate $\mathbf{s}$.

The conditional PDF $p(\mathbf{Y}|\mathbf{s})$ in (35) is the ML metric of the HIHO MSDD. Therefore, based on (42), the detected symbol

vector $\hat{\mathbf{s}}$ will be the vector that satisfies

$$\hat{\mathbf{s}}_{ML} = \arg\max_{\mathbf{s}\in\mathcal{M}^{N_w}} \left(p(\mathbf{Y}|\mathbf{s})\right) \tag{43}$$

$$= \arg\min_{\mathbf{s}\in\mathcal{M}^{N_w}} \left(Tr\left\{\mathbf{Y}^H \Psi^{-1}\mathbf{Y}\right\}\right) \tag{44}$$

$$= \arg\min_{\mathbf{s}\in\mathcal{M}^{N_w}} \left(Tr\left\{\mathbf{Y}^H \,\mathrm{diag}(\mathbf{s})\, \mathbf{C}^{-1}\, \mathrm{diag}(\mathbf{s})^H\, \mathbf{Y}\right\}\right) \tag{45}$$

$$= \arg\min_{\mathbf{s}\in\mathcal{M}^{N_w}} \sum_{p=1}^{P} \left(\mathbf{s}^H \cdot \mathrm{diag}(\mathbf{y}_p) \cdot \mathbf{C}^{-1} \cdot \mathrm{diag}(\mathbf{y}_p)^H \cdot \mathbf{s}\right) \tag{46}$$

$$= \arg\min_{\mathbf{s}\in\mathcal{M}^{N_w}} \sum_{p=1}^{P} \left(\mathbf{s}^H \cdot \mathrm{diag}(\mathbf{y}_p) \cdot \mathbf{F}^H \cdot \mathbf{F} \cdot \mathrm{diag}(\mathbf{y}_p)^H \cdot \mathbf{s}\right), \tag{47}$$

where (40) was used and $\mathbf{F}$ is an upper-triangular matrix obtained by the Cholesky factorization of $\mathbf{C}^{-1}$ and satisfies

$$\mathbf{C}^{-1} = \mathbf{F}^H \mathbf{F}. \tag{48}$$

By defining the upper-triangular matrix $\mathbf{U}_p$ for $p = 1, 2, \ldots, P$ as

$$\mathbf{U}_p \triangleq \mathbf{F}\,\mathrm{diag}(\mathbf{y}_p)^H = \mathbf{F}\,\mathrm{diag}(\mathbf{y}_p)^* \tag{49}$$

and substituting it in (47) we obtain

$$\hat{\mathbf{s}}_{ML} = \arg\min_{\mathbf{s}\in\mathcal{M}^{N_w}} \sum_{p=1}^{P} \left(\mathbf{s}^H \cdot \mathbf{U}_p^H \cdot \mathbf{U}_p \cdot \mathbf{s}\right) \tag{50}$$

$$= \arg\min_{\mathbf{s}\in\mathcal{M}^{N_w}} \sum_{p=1}^{P} \left(\| \mathbf{U}_p \cdot \mathbf{s} \|_2^2 \right). \tag{51}$$

The ML MSDD performs optimally by exhaustively searching the entire set $\mathcal{M}^{N_w-1}$ for the symbol vector $\mathbf{s}$ that satisfies (51). Therefore, the Cost Function (CF) of the HIHO MSDD is

$$f_{MSDD}^{HIHO}(\mathbf{s}) = \sum_{p=1}^{P} \left(\| \mathbf{U}_p \cdot \mathbf{s} \|_2^2 \right). \tag{52}$$

D. MAXIMUM A POSTERIORI PROBABILITY MULTIPLE SYMBOL DIFFERENTIAL DETECTOR [3]

When channel coding is used, the decoding procedure yields improved estimates of the source's bits, especially, when the inputs of the decoder are soft estimates of the encoded bits. Therefore, the MSDDs should provide the decoder these soft estimates by generating extrinsic bit-based or symbol-based LLRs. Moreover, the BER performance of the system is further improved, if information is allowed to be transferred from the decoder to the MSDD, resulting in iterations between the MSDD and the decoder. In this case, the MSDD should be capable of accepting soft inputs in terms of the *a priori* LLRs of the encoded bits. The *a priori* LLRs provided by the decoder affect the calculation of the extrinsic LLR.

Based on (35), (47) and (51), the *a posteriori* LLR of the tth symbol's mth bit, with $t \in \{2, 3, \ldots, N_w\}$ and $m \in \{1, 2, \ldots, \log_2(M_c)\}$, at the output of the MAP MSDD is

$$L_{MSDD,apo}\left(b_t^{(m)}\right) = \ln \frac{P\left(b_t^{(m)} = 0 \mid \mathbf{Y}\right)}{P\left(b_t^{(m)} = 1 \mid \mathbf{Y}\right)} \tag{53}$$

$$= \ln \frac{p\left(\mathbf{Y} \mid b_t^{(m)} = 0\right) \cdot P\left(b_t^{(m)} = 0\right)/p(\mathbf{Y})}{p\left(\mathbf{Y} \mid b_t^{(m)} = 1\right) \cdot P\left(b_t^{(m)} = 1\right)/p(\mathbf{Y})} \tag{54}$$

$$= \ln \frac{\sum_{\mathbf{x}\in\chi(t,m,0)} \exp\left(-Tr\left\{\mathbf{Y}^H\Psi^{-1}\mathbf{Y}\right\} + \ln\left(P(\mathbf{x})\right)\right)}{\sum_{\mathbf{x}\in\chi(t,m,1)} \exp\left(-Tr\left\{\mathbf{Y}^H\Psi^{-1}\mathbf{Y}\right\} + \ln\left(P(\mathbf{x})\right)\right)} \tag{55}$$

$$= \ln \frac{\sum_{\mathbf{x}\in\chi(t,m,0)} \exp\left(-\sum_{p=1}^{P}\left(\| \mathbf{U}_p \cdot \mathbf{s} \|_2^2\right) + \ln\left(P(\mathbf{x})\right)\right)}{\sum_{\mathbf{x}\in\chi(t,m,1)} \exp\left(-\sum_{p=1}^{P}\left(\| \mathbf{U}_p \cdot \mathbf{s} \|_2^2\right) + \ln\left(P(\mathbf{x})\right)\right)}, \tag{56}$$

where $\chi(n, m, v) = \left\{\mathcal{M}^{N_w} \mid b_n^{(m)} = v\right\}$ is the set that includes the specific multi-level symbols of $\mathcal{M}^{N_w}$ of which the $(n \cdot \log_2(M_c) + m)$th bit is equal to v. Furthermore, assuming that the bits of a symbol are independent, the symbol-based *a priori* LLR $P(\mathbf{x})$ is equal to

$$P(\mathbf{x}) = P\left(\mathbf{b}_2^{(1)}\right) \cdots P\left(\mathbf{b}_2^{(\log_2(M_c))}\right) \cdot P\left(\mathbf{b}_3^{(1)}\right) \cdots P\left(\mathbf{b}_{N_w}^{(\log_2(M_c))}\right). \tag{57}$$

The extrinsic LLR of the nth symbol's mth bit is calculated by removing the contribution of the bit-based *a priori* LLR that corresponds to $b_n^{(m)}$, as in

$$L_{m,ex}\left(b_n^{(m)}\right) = L_{m,apo}\left(b_n^{(m)}\right) - \ln\left(\frac{P\left(b_n^{(m)} = 0\right)}{P\left(b_n^{(m)} = 1\right)}\right). \tag{58}$$

The MAP MSDD calculates every additive term in both the numerator and denominator of (55) that takes part in the computation of the extrinsic LLR [3]. The CF in the SISO MSDD is similar to that of the HIHO MSDD and it is extracted from (55) as in

$$f_{MSDD}^{SISO}(\mathbf{x}) = -Tr\left\{\mathbf{Y}^H\Psi^{-1}\mathbf{Y}\right\} + \ln\left(P(\mathbf{x})\right) \tag{59}$$

Therefore, when an M_c-ary modulation scheme is employed and the detection window of the MSDD has a size of N_w symbols, the complexity of the MAP MSDD is equal to

$$\mathcal{C}_{MAP} = \frac{M_c^{N_w-1}}{(N_w-1)\log_2(M_c)}, \tag{60}$$

where $(N_w - 1)$ was used instead of N_w, since the reference symbol is known at the receiver.

III. QUANTUM SEARCH ALGORITHMS

In quantum computing, the equivalent of the classical bit is the quantum bit, or *qubit*.[1] A qubit $|q\rangle$ may be found in the $|0\rangle$ or $|1\rangle$ states, or any superposition of the two, as encapsulated in

$$|q\rangle = a|0\rangle + b|1\rangle, \tag{61}$$

where $a, b \in \mathbb{C}$ and $|a|^2 + |b|^2 = 1$. When we desire to observe a qubit's state, we have to "measure" it on an orthonormal basis. For example, when we measure the qubit in (61) on the computational basis $\{|0\rangle, |1\rangle\}$, we have $|a|^2$ probability of obtaining the state $|0\rangle$ and $|b|^2$ probability of obtaining the state $|1\rangle$. The state of a qubit evolves by passing it through unitary operators. One of the most commonly used unitary operators is the Hadamard operator H, which is defined as:

$$H|0\rangle = \frac{1}{\sqrt{2}}|0\rangle + \frac{1}{\sqrt{2}}|1\rangle = |+\rangle \tag{62}$$

$$H|1\rangle = \frac{1}{\sqrt{2}}|0\rangle - \frac{1}{\sqrt{2}}|1\rangle = |-\rangle. \tag{63}$$

Multiple qubits may form quantum registers, allowing a superposition of a number of states that is exponentially increasing with the number of qubits. For instance, if we have $n = 2$ qubits, they may be found in the following superposition of states:

$$|q_1\rangle|q_2\rangle = a|00\rangle + b|01\rangle + c|10\rangle + d|11\rangle, \tag{64}$$

where $|a|^2+|b|^2+|c|^2+|d|^2 = 1$ and $|c|^2$ is the probability of observing the two qubits in the $|10\rangle$ state. Let us now consider the two qubits in (64), where $a = 1/\sqrt{2}$, $b = 0$, $c = 0$ and $d = 1/\sqrt{2}$, resulting in the quantum state

$$|q_1 q_2\rangle = \frac{|00\rangle + |11\rangle}{\sqrt{2}}. \tag{65}$$

By measuring only the first qubit in (65) we may observe it in the $|0\rangle$ state with 50% probability and in the $|1\rangle$ state with 50% probability. Let us assume that we observe it in the $|1\rangle$ state. Automatically, the second qubit is also in the $|1\rangle$ state with 100% probability. Therefore, the measurement or observation of one of the qubits in (65) affects the state of the other qubit, indicating that the two qubits are *entangled*.

In the context of search, let us refer to the multi-level symbols by stating their respective decimal index representation. For instance, in a system where $U = 2$ users transmit QPSK symbols, the 2-level symbol $\mathbf{x} = \left[(+1+j)/\sqrt{2}, (+1-j)/\sqrt{2}\right]$ is demapped to [00|01] with a decimal representation of $x = 1$. The integration of the quantum algorithms with the QMSDD is depicted in Fig. 5.

[1] A qubit may be interpreted as a spinning coin in a black box, where it is simultaneously in the "Heads" and "Tails" state, until it settles down and we observe it to be either "Heads" or "Tails" after it has settled down. The qubit may be physically implemented using different methods, such as the spin of an electron, the polarization of a photon, or the states of a superconductor [57], [58]. For an extensive tutorial on quantum computing and quantum search algorithms, please refer to [14].

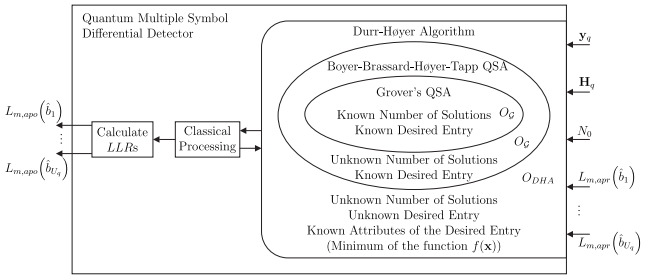

FIGURE 5. The DHA employed in our QMSDDs makes multiple calls to the BBHT QSA. Grover's QSA is not used, but it is included for terms of completion, since the BBHT QSA uses the same Oracle $O_{\mathcal{G}}$, but may even operate when the number of solutions is unknown. The QMSDD is performed on a subcarrier basis. The DHA receives as input the received signals at all the receive AEs on the qth subcarrier, the channel estimates, the noise's variance and the *a priori* LLRs. After it completes its initial procedure, the DHA exchanges information with a classical processing unit, which determines whether the DHA should be called again and its search space. Finally, the QMSDD outputs the calculated *a posteriori* LLRs.

A. GROVER'S QUANTUM SEARCH ALGORITHM

Given a known value δ and an unsorted database representing a function $f(x)$, a search algorithm finds that specific x value, for which we have $f(x) = \delta$ with ∼100%. The index x that corresponds to the known value δ in the database is termed as the *solution* to the search problem. In an N-element database, the classical algorithms require $O(N)$ queries to the database, where $O(\cdot)$ represents the order of a number, while Grover's QSA finds a solution with ∼100% success probability after $O(\sqrt{N})$ calls [31], [32]. However, the number of legitimate solutions S of the search problem has to be known for finding them by Grover's QSA [24], [31].

For an N-element database, Grover's QSA initially employs $n = \log_2 N$ qubits to the $|0\rangle^{\otimes n}$ quantum state.[2] Afterwards, every qubit passes through a Hadamard gate H resulting in the quantum state

$$|x\rangle = \sum_{q=0}^{N-1} \frac{1}{\sqrt{N}}|q\rangle = \sum_{q=0}^{N-1} \frac{1}{\sqrt{M^{N_w-1}}}|q\rangle, \tag{66}$$

as detailed in [31] and [32]. The Grover operator $\mathcal{G} = HP_0H \cdot O_{\mathcal{G}}$ is then applied to the qubits, where H is the Hadamard gate, P_0 is a rotation gate that maps $|x\rangle$ to $-|x\rangle$ if and only if $|x\rangle = |0\rangle^{\otimes n}$, and $O_{\mathcal{G}}$ is the Oracle gate. The Oracle operator $O_{\mathcal{G}}$ evaluates the function for all the inputs that the quantum states are superimposed in and maps $|x_s\rangle \rightarrow -|x_s\rangle$ in (66) for those specific quantum states, which satisfy $f(x_s) = \delta$. The diffusion operator HP_0H then evolves the resultant states in such a way so that the solution states $|x_s\rangle$ have a higher probability to be observed during a potential measurement than the rest of the states. Therefore, after a single application of the Grover operator, the equiprobable superposition of states in (66) is changed to a biased superposition of states in the favour of the solution states.

[2] The n-element tensor product is defined as: $|0\rangle^{\otimes n} = \underbrace{|0\rangle_1 \otimes |0\rangle_2 \otimes \cdots \otimes |0\rangle_n}_{n} = \underbrace{|0\rangle_1|0\rangle_2 \ldots |0\rangle_n}_{n} = \underbrace{|00\ldots0\rangle}_{n}$.

After applying the Grover operator L_{opt} times, where

$$L_{opt} = \left\lceil \frac{\pi}{4}\sqrt{\frac{N}{S}} \right\rceil, \tag{67}$$

the probability of observing the resultant $\mathcal{G}^L|x\rangle$ quantum state and obtaining a solution is given by [31], [32]

$$P_{success} = \sin^2\left[\left(2L_{opt}+1\right)\theta\right], \tag{68}$$

where we have $\theta = \arcsin\left(\sqrt{S/N}\right)$.

The Oracle evaluates the CF once in the Quantum Domain (QD) during every Grover operator. Since the actual complexity of the Oracle will depend on the particular technology used to create it, let us continue by assuming that a single Oracle operation is equivalent to a single CFE in the Classical Domain (CD). In our communications application, the Oracle evaluates the CF of (52) or (59) and therefore a single application of the Oracle is assumed to be equivalent to a single evaluation of the respective CF. The CF of the MSDD does not require the knowledge of the channel states, but it may require extra computations with respect to the CF of the coherent detection schemes, such as the calculation of autocorrelation function of the users' channel states of (28) and the conditional autocorrelation matrix of the Rayleigh channel of (40).

B. BOYER, BRASSARD, HØYER, TAPP QUANTUM SEARCH ALGORITHM

When the number of solutions S is not known, Grover's QSA cannot be employed, since we are unable to calculate the optimal number of Grover iterations in (67). The Boyer, Brassard, Høyer, Tapp (BBHT) QSA [14], [24] employs the Grover operator a pseudo-random number of times, L, and checks whether the outcome is a solution or not, by then evaluating the function in the CD. If the outcome is a solution, then the BBHT QSA outputs it and stops. If it is not, the process is restarted, after updating the set that L takes its values from in Step 2 of Algorithm 1. Finally, if a solution x_s exists, it will have been found with $\sim$100% success probability before

$$L^{QD}_{BBHT} = 4.5\sqrt{N/S} \tag{69}$$

Grover iterations in the QD [24]. The detailed steps of the algorithm are presented in Algorithm 1. Since the number of solutions S is unknown, the worst-case scenario corresponds to $S = 1$, hence the BBHT QSA times out after

$$L^{QD,\max}_{BBHT} = 4.5\sqrt{N} \tag{70}$$

CFEs or database queries, concluding that there is no solution to the search problem.

C. DÜRR - HØYER ALGORITHM

The DHA [21] succeeds in finding the specific index $x_{\min}$ that minimizes the function $f(x)$ or, equivalently, corresponds to the minimum entry in a database with $\sim$100% probability after $O(\sqrt{N})$ CFEs. The steps of the DHA are given in Algorithm 2. Commencing from an initial index $i = x_I$, the DHA employs the BBHT QSA in conjunction with an alternative Oracle. More specifically, the DHA's Oracle marks as solutions all the specific states x that satisfy $f(x) < f(i)$. After the call to the BBHT QSA ends, a x_s has been found, where we have $f(x_s) < f(i)$. After making $i = x_s$, the BBHT QSA is called again for finding another x_s that corresponds to an even smaller CF value. This process is continued until the BBHT QSA concludes that there is no solution to the search problem, essentially indicating that $x_{\min}$ was found during the last call to the BBHT QSA. The choice of the initial index x_I was shown to be related to the complexity of the algorithm [12], [14]. The maximum number of CFEs performed in the QD required by the DHA to find $x_{\min}$ is equal to [21]

$$L^{QD,\max}_{DHA} = 22.5\sqrt{N}, \tag{71}$$

while the minimum number of CFEs performed in the CD when the BBHT QSA evaluates the observed state in the CD

Algorithm 1 Improved BBHT-QSA [63]

1: Set $m \leftarrow 1$, $\lambda \leftarrow 6/5$ and $L^{QD}_{BBHT} \leftarrow 0$, $L^{CD}_{BBHT} \leftarrow 0$.
2: Choose L uniformly from the set $\{0, \ldots, \lfloor m \rfloor\}$.
3: Apply the $\mathcal{G}$ operator L times starting from the initial state $|x\rangle$ in (66), resulting in the final state $|x_f\rangle = \mathcal{G}^L|x\rangle$.
4: Observe $|x_f\rangle$ in the QD and obtain $|j\rangle$.
5: Compute $f(x)$ in the CD.
6: Update $L^{CD}_{BBHT} \leftarrow L^{CD}_{BBHT} + 1$ and $L^{QD}_{BBHT} \leftarrow L^{QD}_{BBHT} + L$.
7: **if** $f(x) = \delta$ or $L^{QD}_{BBHT} \geq L^{QD,\max}_{BBHT}$ **then**
8: Set $x_s \leftarrow j$, output x_s, L^{CD}_{BBHT}, L^{QD}_{BBHT} and exit.
9: **else**
10: Set $m \leftarrow \min\left\{\lambda m, \sqrt{N}\right\}$.
11: **if** $m = \sqrt{N}$ **then**
12: Choose L uniformly from the set $\{1, \ldots, \lfloor m \rfloor\}$ and go to step 4.
13: **else**
14: Go to step 3.
15: **end if**
16: **end if**

Algorithm 2 Deterministically-Initialised DHA [12], [13]

1: Set $i \leftarrow x_I$ and $L_{DHA} \leftarrow 0$, $L^{CD}_{DHA} \leftarrow 0$, $L^{QD}_{DHA} \leftarrow 0$.
2: The BBHT QSA is employed with $\delta \leftarrow f(i)$, an Oracle that marks as solutions the states $|x\rangle$ that obey $f(x) < \delta$ and $L^{QD,\max}_{BBHT} \leftarrow 4.5\sqrt{N}$. Obtain x_s, L^{CD}_{BBHT} and L^{QD}_{BBHT} from the BBHT QSA.
3: $L^{CD}_{DHA} \leftarrow L^{CD}_{DHA} + L^{CD}_{BBHT}$, $L^{QD}_{DHA} \leftarrow L^{QD}_{DHA} + L^{QD}_{BBHT}$ and $L_{DHA} \leftarrow L_{DHA} + L^{CD}_{DHA} + L^{QD}_{DHA}$.
4: **if** $f(x_s) \geq f(i)$ or $L_{DHA} \geq 22.5\sqrt{N}$, **then**
5: Set $x_{\min} \leftarrow i$, output $x_{\min}$ and exit.
6: **else**
7: Set $i \leftarrow x_s$ and go to Step 2.
8: **end if**

for checking if it is a solution is [13]

$$L_{DHA}^{CD,\,\min} = \min\left(L_{DHA}^{CD}\right)+1 \quad s.t. \left[\sum_{j=0}^{L_{DHA}^{CD}-1} \min\left(\left\lfloor \lambda^j \right\rfloor, \sqrt{N}\right)\right] \geq 4.5\sqrt{N}. \quad (72)$$

IV. QUANTUM-ASSISTED MULTIPLE SYMBOL DIFFERENTIAL DETECTION

In this section we present the proposed QMSDDs in the uplink of a $U = 4$-user DSS/SSCH SDMA-OFDM system relying on a single transmit antenna each and $P = 2$ receive AEs at the BS, using QPSK modulation, Turbo Coding (TC) with $R = 1/2$ rate and 8 Trellis states, as well as $Q = 1024$ subcarriers with a channel bandwidth of 10 MHz [64]. In contrast to the LTE standard, we will assume that all $Q = 1024$ subcarriers are active. Moreover, each user transmits on $W = 512$ subcarriers out of the available $Q = 1024$ subcarriers and is allocated one of the $G = 2$ available Walsh-Hadamard DSS codes. The schedule of the subcarrier allocation is generated by the DSS-based USSCH [13] and it changes every $T_h = 13$ OFDM symbol periods, while the length of a symbol frame is equal to 12 288 symbols. Let us use the Extended Pedestrian A (EPA) LTE channel model [64] for our example. The parameters of the system are described in Table 1. The sampling frequency is chosen according to the LTE standard [64], while a carrier frequency of $f_c = 2.5$ GHz is selected. The mobile velocity of the EPA channel is the one that corresponds to the maximum Doppler frequency of the channel, according to the LTE standard [64]. All the channels are assumed to experience Rayleigh fading. The Rayleigh fading is a complex-valued zero-mean Gaussian process with a variance of σ_h^2 [3].

A. DÜRR-HØYER ALGORITHM-BASED QMSDD

The DHA may be used for performing HIHO QMSDD. The CF of the HIHO differential detection is stated in (51). The effective search space has

$$\mathcal{C}_{ML} = M^{N_w-1} \quad (73)$$

entries and hence the complexity of the ML MSDD increases exponentially with the size of the detection window $2 \leq N_w \leq T_h$, requiring M^{N_w-1} CFEs. The HIHO MSDD's CF is evaluated by the Oracle and accordingly, the DHA QMSDD succeeds in finding that specific symbol vector $\mathbf{s}$, which minimizes the CF in (51) at a complexity of $O\left(\sqrt{M^{N_w-1}}\right)$ CFEs. Let us initially assume that the DHA QMSDD is randomly initialized.

Let us proceed by comparing the DHA QMSDD to both the ML MSDD and to the CDD in our DSS/SSCH SDMA-OFDM system characterized in Table 1. The size of the detection window N_w is chosen to be $N_w = 5$ or $N_w = 7$, where $N_w = 2$ corresponds to an MSDD equivalent to the CDD. The symbol detected by the MSDDs at the N_wth position of $\mathbf{s}$ is the reference symbol of the subsequent MSDD procedure.

TABLE 1. Parameters of the 4-user OFDM system.

Number of Users	$U = 4$
Number of AEs per User	$N_{T_x} = 1$
Number of AEs at the BS	$P = 2$
Normalized User Load	$U_L = U \cdot N_{T_x}/P = 2$
Modulation	DQPSK in time domain
Channel Code	Turbo Code, $R = 1/2$,
	8 Trellis states
	$I_{inner} = 4$ iterations
Number of Subcarriers	$Q = 1024$
Cyclic Prefix	CP = 128
Number of Subcarriers per User	$W = 512$
Number of WH DSS Codes	$G = 2$
Subcarrier Allocation every	$T_h = 13$ OFDM symbol periods
Bit Interleaver Length	24 576 per User
Sampling Frequency	$f_s = 15.36$ MHz
Carrier Frequency	$f_c = 2.5$ GHz
Extended Pedestrian A (EPA)	
Mobile Velocity	$v = 5$ km/h
Normalized Doppler Frequency	$f_d = 7.54 \cdot 10^{-7}$
Number of Taps	$N_{taps} = 5$
Power Profile	$[-2.392,\ -4.392,\ -12.931,$
	$-22.131,\ -25.731]$
Delay Profile	[0 1 2 3 6]

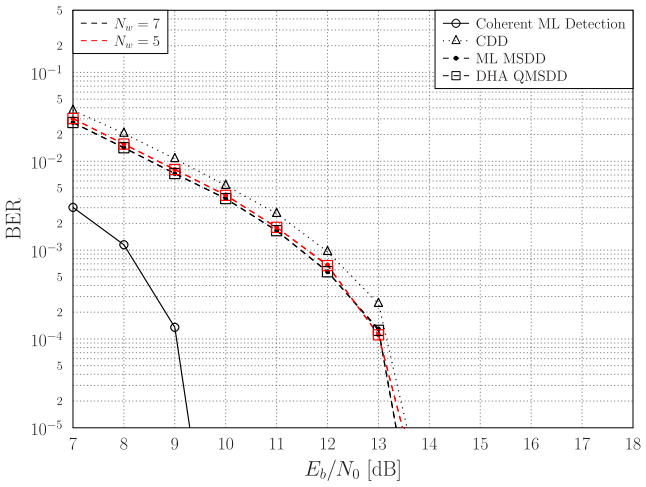

FIGURE 6. BER performance of the DHA QMSDD, the ML MSDD and the CDD in the DSS/SSCH SDMA-OFDM system of Fig. 3, using the parameters summarized in Table 1. The BER performance of the coherent detection of the same system is also included for comparison.

Fig. 6 depicts the BER performance of both the DHA QMSDD, as well as of the ML MSDD and of the CDD in our system scenario. Additionally, we have included the performance of the equivalent coherent system for reference, where the channel states have been perfectly estimated at the BS. We may observe that the DHA QMSDD has an equivalent

TABLE 2. Computational complexity in terms of the number of CFEs/bit in Fig. 6.

	$N_w = 5$	$N_w = 7$
ML MSDD	32 CFEs / bit	341.33 CFEs / bit
DHA MSDD	12.77 CFEs / bit	43.6 CFEs / bit

performance to that of the ML MSDD, for both values of N_w. At the same time, the computational complexity of the DHA QMSDD was only 55% and 12.77% of the corresponding complexities of the ML MSDD for $N_w = 5$ and $N_w = 7$, respectively, as presented in Table 2. Furthermore, the ML MSDD and the DHA QMSDD perform better than the CDD by approximately 0.6 dB for $N_w = 7$. Naturally, the BER versus Signal to Noise Ratio (SNR) improvement is achieved at an increased complexity, since the complexity of the CDD is 2 CFEs / bit. The BER improvement between the scenario where $N_w = 7$ was used and the one where $N_w = 5$ was selected is 0.2 dB. This is mainly due to the fact that since we have $T_h = 13$, there are two and three detection windows when $N_w = 7$ and $N_w = 5$, respectively, resulting in a similar performance. The expected 3 dB difference between the coherent ML detection and the MSDDs is indeed present in Fig. 6 and it becomes higher upon increasing E_b/N_0 due to the channel coding having a more beneficial effect on coherent systems [3].

B. EARLY-STOPPING AIDED DHA-BASED QMSDD

The ES-DHA was proposed in [12]. Based on the acquired statistics of the required number of CFEs of off-line searches using the DHA, the ES-DHA may be able to reduce the necessary complexity of the QMSDD. In more detail, when the randomly-initialised or the deterministically-initialised DHA finds the symbol vector $\hat{\mathbf{s}}_{ML}$ of (51) after a number of BBHT iterations, it does not realize this success until another BBHT iteration yields a symbol vector $\mathbf{s}$, which has a higher CF value than that of the already found $\hat{\mathbf{s}}_{ML}$. By simulating a large number of DHA searches in an off-line fashion for the same search space size as our system's search space, we may gather statistics concerning the number of CFEs that were required for the DHA to find the solution $\hat{\mathbf{s}}_{ML}$, rather than to realize that the solution has already been found [12]. By carefully interpreting these statistics, we are able to perform optimal MSDD at a reduced complexity, or allow a suboptimal performance, if we operate under a strict complexity-budget in terms of the number of CFEs.

For our scenario, the CDF curves of the number of CFEs performed both in the CD and the QD, as well as the total number of CFEs carried out in both domains during the DHA searches are plotted in Fig. 7a for $N_w = 7$ and $E_b/N_0 = 13.5$. Since the initial DHA input is selected to be random, the value of the E_b/N_0 does not affect the resultant PDF and CDF curves [12]. We simulated the DHA in our system scenario for $12 \cdot 10^6$ independent instances. Fig. 7a shows that in 99% of the DHA instances, the search was completed in

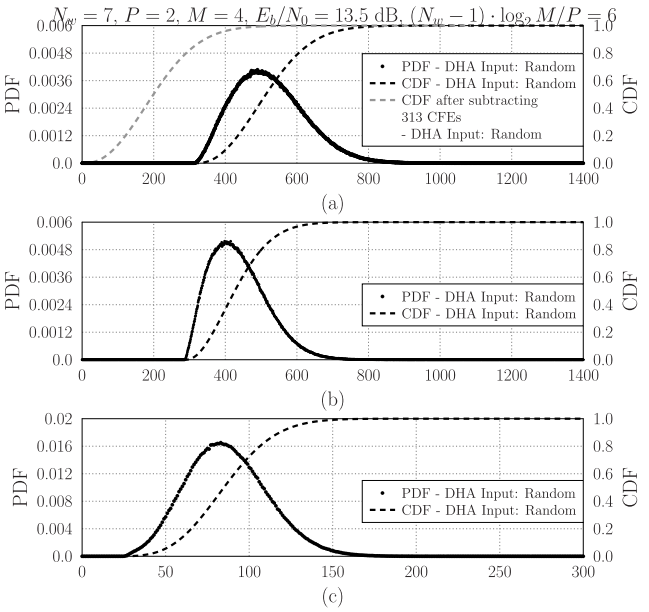

FIGURE 7. PDF and CDF curves of the DHA in the system scenario of Fig. 3, using the parameters summarized in Table 1 for $N_w = 7$ after $12 \cdot 10^6$ number of independent DHA instances, before and after subtracting the minimum total number of CFEs, equal to 314 CFEs, required by the DHA to realize that the solution has already been found. (a) Total number of CF evaluations. (b) Number of Grover iterations (CF evaluations in the QD). (c) Number of CF evaluations in the CD.

fewer than 787 CFEs, or performing less than $787/4096 \cdot 100\% = 19.2\%$ of the number of CFEs required by the ML QMSDD. Similarly, 80% of the DHA searches were completed after evaluating the CF of (51) at most 605 times, which forms 14.8% of the number of CFEs per multi-level MSDD symbol vector performed in the ML MSDDs. It should be noted at this point that the statistics do not take into consideration the success of the search, but only the complexity required for the search to be completed. However, the DHA has a success probability of ∼100%, hence in most of the instances the search is indeed successful. By exploiting the CDF curves of Fig. 7 we may stop the DHA in our scenario after 787 CFEs and expect a ∼99% success probability in our search for $\hat{\mathbf{s}}_{ML}$.

By observing Fig. 7a we are also able to infer that the minimum number of total CFEs required by the DHA to complete its actions is 313, which forms 7.6% of the CFEs in the ML MSDD. This is the minimum number of CFEs that the DHA required out of $12 \cdot 10^6$ instances for realizing that it had already found $\hat{\mathbf{s}}_{ML}$ and this corresponds to the scenario, where the random initial DHA input was equal to $\hat{\mathbf{s}}_{ML}$ and the minimum number of CFEs both in the CD and the QD were performed. The probability of the random initial DHA input to be equal to the optimal symbol index and at the same time the DHA to require exactly $4.5\sqrt{M_c^{N_w-1}} = 288$ CFEs in the QD for finding it turned out to be equal to $1.4 \cdot 10^{-5}$ based on the CDF seen in Fig. 7b. Furthermore, the minimum number of CFEs performed in the CD was equal to 25 CFEs with a probability of occurrence equal to $9 \cdot 10^{-6}$ according to the CDF in Fig. 7c. In total, the scenario

associated with the lowest complexity is the one, where the random initial DHA input is equal to the optimal symbol index and the DHA performs 288 CFEs in the QD and 25 CFEs in the CD, resulting in a total of 313 CFEs. In our simulation instances this incident occurred with a probability of $3 \cdot 10^{-6}$.

These 313 CFEs did not impact the output, since the initial DHA input was already equal to the desired output. Therefore, the ES-DHA QMSDD considers this amount of 313 CFEs as unnecessary complexity and always subtracts it from the affordable number of CFEs of the DHA, without altering the success probability indicated by the CDF curves. In other words, if we allow the DHA to run in our system scenario for 787 CFEs and for $787-313=474$ CFEs, which form only 11.6% of the number of CFEs performed in the ML MSDD, we should expect a ∼99% success probability in both scenarios. This non-intuitive phenomenon may be logically interpreted as the difference between the number of CFEs the DHA requires to find the solution and the number of CFEs the DHA requires to realize that it has already found the solution. In the first case, the DHA will naturally terminate its own operation 99% of the time while having found the solution. By contrast, in the second case the DHA will naturally stop on its own 34.4% of the time but it will again have found the solution 99% of the time, assuming a 100% success ratio. Fig. 7a also presents the CDF curve after 313 CFEs have been subtracted.

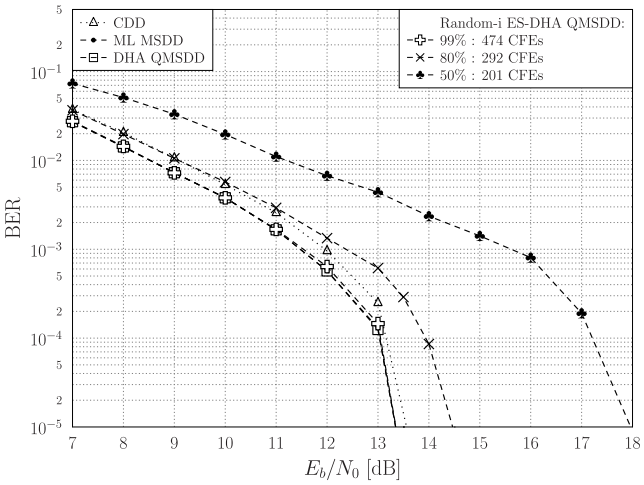

FIGURE 8. BER performance of the ES-DHA QMSDD for the 99%, 80% and 50% points of the CDF curve in Fig. 7, corresponding to a maximum of 474, 292 and 201 CFEs, respectively, in the DSS/SSCH SDMA-OFDM system scenario of Fig. 3, using the parameters summarized in Table 1 for $N_w = 7$.

The BER performance of the ES-DHA QMSDD is illustrated in Fig. 8, where it is compared to the DHA QMSDD of Section IV-A for various early stopping points based on the gray CDF curve in Fig. 7a and $N_w = 7$. According to Fig. 8, the BER performance of the ES-DHA QMSDD when the 474 CFEs corresponding to the 99% point of the CDF are chosen as the maximum affordable number of CFEs is equivalent to that of the DHA QMSDD and the ML MSDD. The computational complexity of the ES-DHA-99% QMSDD is equal to 37.9 CFEs per bit, compared to the complexity of the DHA QMSDD, which requires 43.6 CFEs per bit, according to Table 3. Moreover, when the 80% point of the CDF is selected, the ES-DHA QMSDD's performance is equivalent to that of the CDD until the $E_b/N_0 = 9$ dB point, after which it becomes worse. It seems that in this system scenario, the CDD finds the optimal solution more often than 80% of the time. This might have been expected, since the power gain of the MSDD when compared to the CDD is only 0.5 dB. Similarly, the performance of the ES-DHA QMSDD when the 50% point of the CDF in Fig. 7 is chosen is worse than that of the CDD by $2-3$ dB. The reason for this is that the 201 CFEs in the ES-DHA QMSDD, which correspond to the 50% CDF point, are insufficient for achieving an acceptable performance. Furthermore, the fact that the ES-DHA is randomly-initialized contributes to the fact of experiencing a worse performance than the CDD, when the number of maximum affordable CFEs is not sufficiently high. We will propose a method for circumventing this problem in Section V.

TABLE 3. Complexity in terms of the number of CFEs/bit in Fig. 8.

MSDD	Number of CFEs per bit		
CDD	2		
ML	341.33		
DHA	43.6		
ES-DHA	CDF %	Total CFEs	Number of CFEs per bit (% of CFEs in ML MSDD)
	99%	474	37.9 (11.6%)
	80%	292	24.33 (7.1%)
	50%	201	16.75 (4.9%)

C. DHA-BASED QMSDD WITH MAXIMUM APPROXIMATION

As in the MAP MSDD analysis, let us focus our discussions on the calculation of the tth differentially encoded symbol's mth bit. The methodology of the DHA-based detector relying on the MAximum Approximation (DHA-MAA) is described in detail in [13]. In this section we will apply the DHA-MAA algorithm for performing HISO QMSDD. The DHA-MAA QMSDD calculates the bit-based or symbol-based LLRs by using only a reduced subset of the legitimate multi-level MSDD symbol vectors in the MAP MSDD.

The DHA-MAA QMSDD invokes the DHA for finding the symbol vector $\hat{\mathbf{x}}_{\min}$ that satisfies

$$\hat{\mathbf{x}}_{\min} = \arg\max_{\mathbf{x}\in\mathcal{M}^{N_w-1}} \left\{ \exp\left(-Tr\left\{\mathbf{Y}^H \Psi^{-1} \mathbf{Y}\right\} + \ln\left(P(\mathbf{x})\right)\right)\right\}$$
$$= \arg\min_{\mathbf{x}\in\mathcal{M}^{N_w-1}} \left\{ \sum_{p=1}^{P} \left(\| \mathbf{U}_p \cdot \mathbf{s} \|_2^2 \right) - \ln\left(P(\mathbf{x})\right)\right\}, \quad (74)$$

where the connection between $\mathbf{s}$ and $\mathbf{x}$ is stated in (1) and its CF is given by:

$$f_{MSDD}^{SISO-DHA}(\mathbf{x}) = \sum_{p=1}^{P} \left[\left(\| \mathbf{U}_p \cdot \mathbf{s} \|_2^2 \right) - \ln(P(\mathbf{x})) \right]. \quad (75)$$

The DHA will search through the entire legitimate search space $\mathcal{M}^{N_w-1}$, where the first symbol in the MSDD symbol vector $\mathbf{x}$ is fixed to its known value, since it corresponds to the reference symbol. During the search for $\hat{\mathbf{x}}$, the DHA evaluates the CF value of (75) for many other multi-level symbols, which may be stored and exploited for the calculation of the LLRs. More precisely, once the search is completed, the best symbol found for the numerator and the best symbol found for the denominator of each bit's LLR are used for its calculation. Let us redefine a number of sets for assisting us in the analysis of the DHA-MAA QMSDD. The set $\mathcal{X}$ includes the unique symbols that were evaluated during the DHA search. From that set $\mathcal{X}$, we may then create two sets for each bit, based on the bit's specific value. For example, $\mathcal{X}^{t,m,\mathrm{v}}$ is that particular set, which contains all the symbols in $\mathcal{X}$, where the value of the tth transmitted symbol's mth bit is equal to v. By using the decimal representation x for indexing the corresponding symbol vector $\mathbf{x}$ as in Section III, we have

$$x \in \mathcal{X}^{t,m,\mathrm{v}} \Leftrightarrow x \in \mathcal{X} \wedge \mathbf{x} \in \chi(t, m, \mathrm{v}). \quad (76)$$

In other words, $\mathcal{X}^{t,m,\mathrm{v}}$ includes all the unique symbols that the DHA search encountered, which have the $(t \cdot \log_2 M_c + m)$th bit of their binary representation equal to v. Hence, the LLR calculated by the DHA-MAA is equal to

$$L_{DHA-MAA,apo}\left(b_t^{(m)}\right) = \ln \frac{\max\left(\exp\left(-f_{MSDD}^{SISO-DHA}(x)\right) \mid x \in \mathcal{X}^{t,m,0}\right)}{\max\left(\exp\left(-f_{MSDD}^{SISO-DHA}(x)\right) \mid x \in \mathcal{X}^{t,m,1}\right)}. \quad (77)$$

According to (77), the globally optimal symbol $\hat{\mathbf{x}}$ that is found during the DHA search, will be used for the calculation of every bit's LLR, either in its numerator or in its denominator, since there is no symbol with a higher $\exp\left(-f_{MSDD}^{SISO-DHA}(x)\right)$ value than $\hat{x}_{\min}$. Hence, the signs of the LLRs calculated by the DHA-MAA QMSDD always match the signs of the LLRs calculated by the MAP MSDD. The difference between the two MSDDs' LLRs is in the magnitude of the LLRs, with the DHA-MAA QMSDD tending to output LLRs having a higher confidence than they actually have [13]. This occurs due to the fact that the optimal multi-level symbol of a set is used for the calculation of either the numerator or the denominator, while in some cases a sub-optimal symbol is used for the calculation of the denominator or the numerator, respectively.

In the case when a set $\mathcal{X}^{t,m,\mathrm{v}}$ is empty for a specific $\{t, m, \mathrm{v}\}$ set, the DHA is called again to search for the specific multi-level symbol $\hat{\mathbf{x}}_{\min}^{t,m,v} \in \chi(t, m, \mathrm{v})$ that minimizes the CF in (74) [13]. By employing another DHA search, we can ensure that the optimal symbol of that set is found with ~100% probability and considering that the globally optimal symbol was found during the initial DHA search, the value of the $(t \cdot \log_2 M_c + m)$th bit's LLR calculated by the DHA-MAA QMSDD will be close to that of the MAP MSDD. However, the additional complexity imposed by the extra DHA search is added to the total complexity of the DHA-MAA QMSDD. For this reason, we have proposed in [13] a solution that we termed as the Neighbour Exploitation (NE) technique.

Briefly, according to the NE technique, if the set $\mathcal{X}^{t,m,\mathrm{v}}$ is empty after the initial DHA search, then the neighbour of the globally optimal symbol $\hat{\mathbf{x}}$ that was found at the $(t \cdot \log_2 M_c + m)$th position becomes the sole member of $\mathcal{X}^{t,m,\mathrm{v}}$. More specifically, if the set $\mathcal{X}^{t,m,\mathrm{v}}$ is empty, then the set $\mathcal{X}^{t,m,\mathrm{v}\oplus 1}$ includes $\hat{\mathbf{x}}$. At the price of an additional CFE, we may use the globally optimal symbol $\hat{\mathbf{x}}$ and the corresponding neighbour of $\hat{\mathbf{x}}$ for the calculation of the tth symbol's mth bit's LLR.

The minimum complexity per bit quantified in terms of the number of CFEs of the DHA-MAA QMSDD then becomes [13]

$$\mathcal{C}_{DHA-MAA}^{\min} = \frac{4.5\sqrt{M_c^{(N_w-1)}} + L_{DHA}^{CD,\min}}{(N_w - 1) \cdot \log_2 M_c}, \quad (78)$$

where $L_{DHA}^{CD,\min}$ is the minimum possible number of CFEs performed in the classic domain during the initial DHA search, which is described in (72). By contrast, the minimum number of CFEs of the DHA-MAA-NE QMSDD is equal to [13]

$$\mathcal{C}_{DHA-MAA-NE}^{\min} = \frac{4.5\sqrt{M_c^{(N_w-1)}} + L_{DHA}^{CD,\min}}{(N_w - 1) \cdot \log_2 M_c} + 1, \quad (79)$$

which is only a single CFE higher than the minimum complexity of the DHA-MAA QMSDD in (78) due to the requirements of the NE technique.

In Fig. 9 we compare the BER performances of the MAP MSDD and the DHA-MAA QMSDD both with and without the NE technique, when used in the DSS/SSCH

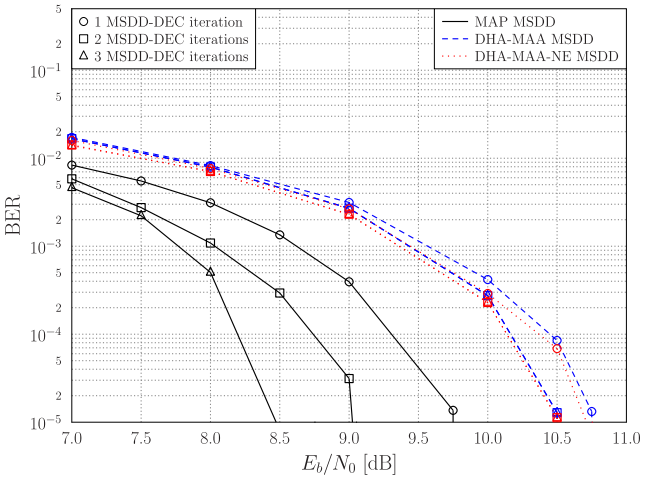

FIGURE 9. BER performance of the DHA-MAA QMSDDs and the MAP MSDD in the DSS/SSCH SDMA-OFDM system scenario of Fig. 3, using the parameters summarized in Table 1 for $N_w = 7$.

SDMA-OFDM system scenario of Fig. 3 relying on the parameters of Table 1 involving $J = 3$ iterations between the MSDD and the channel decoder. We may observe that there is an 1 dB loss between the MAP MSDD and the DHA-MAA QMSDD with 1 MSDD-DEC iteration. Additionally, the DHA-MAA-NE QMSDD offers a slightly better BER performance, when compared to that of the DHA-MAA QMSDD. When the number of iterations between the MSDDs and the decoders is increased, the performance of the MAP MSDD is improved, but those of the DHA-MAA QMSDD and the DHA-MAA-NE QMSDD essentially remain the same, hence resulting in a power loss of approximately 2 dB for the latter pair after $J = 3$ MSDD-DEC iterations between the MAP MSDD and the DHA-MAA QMSDDs.

The computational complexities of the MSDDs quantified in terms of the number of CFEs per bit are summarized in Table 4, where again the CF is given in (75). We make the conclusive assumption that all the CF values obtained by the MAP MSDD during the first MSDD-DEC iteration are stored and reused during any subsequent iterations, which reduces the complexity. Therefore, the complexity of the MAP MSDD is assumed to be independent of the number of MSDD-DEC iterations, when quantified in terms of the number of CFEs. On the other hand, we assume that the DHA-MAA QMSDD is performed during every MSDD-DEC iteration. In this way, the comparison of the complexities of the classical and quantum MSDDs has the smallest difference possible and corresponds to the worst-case-scenario for the QMSDDs.

TABLE 4. Complexity in terms of the number of CFEs/bit in Fig. 9.

MSDD / QMSDD	$E_b/N_0 = 10.5$ dB		
	Number of MSDD-DEC iterations		
	1	2	3
MAP	341.33	341.33	341.33
DHA-MAA	43.70	44.13	44.57
DHA-MAA-NE	44.62	45.95	46.26
MSDD / QMSDD	$E_b/N_0 = 5$ dB		
	Number of MSDD-DEC iterations		
	1	2	3
MAP	341.33	341.33	341.33
DHA-MAA	43.70	88.53	128.05
DHA-MAA-NE	44.62	88.34	130.73

According to Table 4, the complexities of the DHA-MAA and DHA-MAA QMSDDs are lower than that of the MAP MSDD. When operating at $E_b/N_0 = 10.5$ dB the complexity of the QMSDDs does not increase dramatically with the number of MSDD-DEC iterations, because most of the time the entire frame was correctly decoded during the first iteration. Therefore, the small number of additional CFEs, which may be as low as a single CFE per bit, when $J = 2$ MSDD-DEC iterations are performed, provides a modest gain of 0.25 dB as observed in Fig. 9, when we compare the QMSDDs using $J = 1$ MSDD-DEC iteration and that using $J = 2$ MSDD-DEC iterations. Similarly, when $J = 3$ iterations are allowed between the MSDDs and the channel decoders, the complexities of the QMSDDs are only slightly increased at $E_b/N_0 = 10.5$ dB. However, the BER performance remains essentially the same as in the case, where $J = 2$ MSDD-DEC iterations were performed. When we have $E_b/N_0 = 5$ dB, the complexities of the DHA-MAA QMSDDs combined with multiple MSDD-DEC iterations may be deemed to be the corresponding multiples of the complexities required for a single MSDD-DEC iteration. For example, in the case of the DHA-MAA-NE QMSDD, 44.62 CFEs are required for a single MSDD-DEC iteration, while almost three times more are necessitated for the scenario where $J = 3$ MSDD-DEC iterations are performed. Observe in Fig. 9 this increased complexity fails to achieve any substantial BER performance improvement for the system. The reason for the increase in complexity is that none of the frames are correctly decoded during any of the previous iterations.

Therefore, based on Fig. 9, despite increasing the receiver-complexity by allowing iterations between the MSDD and the channel decoder, the performance of the DHA-MAA QMSDDs is not improved. In the context of the DHA-MAA QMSDD, the MSDD-DEC iterations translate into updated values of the *a priori* symbol-based probabilities $P(\mathbf{x})$ in (55) and (74). By calculating the LLR as in (77), the DHA-MAA QMSDD essentially ignores other symbols, although they would be expected to improve the resultant LLR value. Moreover, since the DHA-MAA QMSDD does not always use the optimal symbols for the calculation of both the numerator and the denominator of each bit's LLR, the excessive value of the resultant LLRs, which actually represent an undue confidence, have a negative effect on the channel decoder by misinforming it. This is verified by observing the EXIT chart of our system scenario in Fig. 10, where the inner decoder's curves corresponding to the MSDDs and the outer decoder's curve corresponding to the TC employed are depicted. Furthermore, the Monte-Carlo simulation based stair-case-shaped decoding trajectories were generated for a frame length of 24 576 bits per user. All the EXIT curves in this treatise have been generated by using the histogram-based method [3], which provides more accurate predictions of the soft-information PDFs than the Gaussian approximation.

According to Fig. 10, the DHA-MAA and DHA-MAA-NE QMSDDs initially output a lower MI than the MAP MSDD, but upon iterating they eventually become higher than that of the MAP MSDD, yielding a higher MI at their output. This fact does not represent the reality, yet, it was expected. The DHA-MAA and DHA-MAA-NE QMSDD always generate extrinsic LLRs, which have the same polarity as the ones the MAP MSDD generates. Due to the fact that the two QMSDDs generate their LLRs according to (77) and that most of the times they do not use the optimal symbols for both

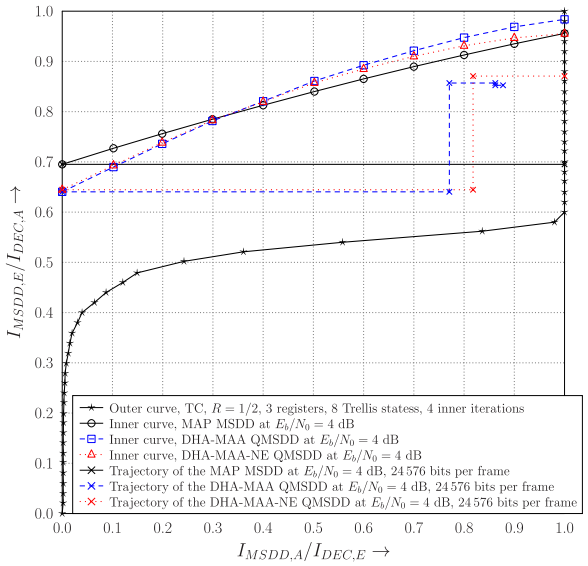

FIGURE 10. EXIT chart of the DHA-MAA and DHA-MAA-NE QMSDDs, as well as the MAP MSDD in the DSS/SSCH SDMA-OFDM system scenario of Fig. 3, using the parameters summarized in Table 1 for $N_W = 7$.

the numerator and the denominator, we expect to obtain LLR values having the correct polarity, but higher values than they should truly have. Therefore, their inner decoder EXIT curves erroneously represent the belief that the QMSDDs surpass the performance of the MAP MSDD.

All the EXIT curves in Fig. 10 have been generated using Gaussian-distributed LLRs as their inputs. The generation of non-Gaussian EXIT charts [65] may provide a more accurate design of a system, especially when approximations in the calculation of the LLRs are used. Nonetheless, in this paper we rely on Gaussian LLR-assumption, for avoiding the related complex discussions.

As a result of this Gaussian approximation, the decoding trajectories of the QMSDDs reach their respective inner decoder curve at $I_{A,MSDD} = 0$, but beyond this point they do not match with their respective EXIT curves. More specifically, the decoding trajectory of the DHA-MAA QMSDD fails to reach the $I_{DEC,E} = 1$ line of perfect convergence to a vanishingly low BER, when the inner and outer decoders are serially connected as in our scenario. The reasons for the behaviour of this trajectory is that the DHA-MAA and DHA-MAA-NE QMSDDs do not satisfy the consistency condition [66], which implies that they provide excessive, overconfident LLR values, which is partly attributable to the fact that their interleaver length is limited to 24 576 bits for each user. If the non-Gaussian EXIT charts [65] were shown, the inner and outer decoder EXIT curves after two and three iterations would form a much narrower tunnel or a closed tunnel, for the DHA-MAA-NE and DHA-MAA QMSDDs, respectively.

D. DHA-BASED QMSDD WITH MULTI-INPUT APPROXIMATION

The Dürr-Høyer algorithm-based MUD with MUA was analysed in [13]. The same principles are followed here for the creation of the DHA-MUA QMSDD. The DHA-MUA QMSDD starts by performing a single DHA search for finding the optimal multi-level MSDD symbol vector that belongs to the numerator of the first bit's LLR and another single DHA search for finding the optimal multi-level symbol that belongs to the denominator of the first bit's LLR. Therefore, the search space of each of the first two DHA searches has M^{N_w-2} entries. The CF used for determining the optimality of the symbols is the one formulated in (75).

When we randomly initialize the DHA-MUA QMSDD, if the randomly selected initial symbol belongs to the numerator of the first bit's LLR, we firstly perform the DHA search for that numerator. Similarly, we commence with the denominator of the first bit's LLR, provided that the random initial symbol belongs to it. Let us assume that we start by performing the DHA for the numerator. After we find the optimal symbol $\hat{\mathbf{x}}_{\min}^{1,1,0}$ in the $\mathcal{X}^{1,1,0}$ set, we initialize the DHA search for the denominator using the neighbour of $\hat{\mathbf{x}}_{\min}^{t,m,0}$ in the first bit position. Once both searches have been completed, we compare the two optimal symbols $\hat{\mathbf{x}}_{\min}^{1,1,0}$ and $\hat{\mathbf{x}}_{\min}^{1,1,1}$ for determining the globally optimal symbol $\hat{\mathbf{x}}_{\min}$ with the aid of:

$$\hat{\mathbf{x}}_{\min} = \begin{cases} \hat{\mathbf{x}}_{\min}^{1,1,0} & \text{if } f_{DHA}\left(\hat{\mathbf{x}}_{\min}^{1,1,0}\right) < f_{DHA}\left(\hat{\mathbf{x}}_{\min}^{1,1,1}\right) \\ \hat{\mathbf{x}}_{\min}^{1,1,1} & \text{if } f_{DHA}\left(\hat{\mathbf{x}}_{\min}^{1,1,0}\right) > f_{DHA}\left(\hat{\mathbf{x}}_{\min}^{1,1,1}\right). \end{cases} \tag{80}$$

For the calculation of the LLRs of the subsequent bits, we only perform a single DHA search per bit. More specifically, if the globally optimal symbol $\hat{\mathbf{x}}_{\min}$ belongs to the numerator of a bit's LLR, then we perform a DHA search for the specific search space that corresponds to the denominator of that bit's LLR, and vice versa. At the end, every set $\mathcal{X}^{t,m,\mathrm{v}}$ for $t \in \{1, 2, \ldots, N_w - 1\}$, $m \in \{1, 2, \ldots, \log_2 M_c\}$ and $\mathrm{v} \in \{0, 1\}$ will contain at least one symbol. Let us assume without loss of generality that the symbols both in $\mathcal{X}^{t,m,0}$ and $\mathcal{X}^{t,m,1}$ are stored in a descending order based on their CF values. The pair of knowledge transfer techniques that were investigated in [13] in the context of MUDs, namely the Forward Knowledge Transfer (FKT)[3] and the Forward and Backward Knowledge Transfer (FBKT)[4], may be readily applied in the context of the QMSDD for the creation of

[3]In the DHA-MUA QMSDD, the search results obtained for the $[(u-1)\cdot\log_2(M)+m]$th bit of a multi-level QMSDD symbol vector on the qth subcarrier are stored in $\mathcal{X}_q^{u,m,0}$ and $\mathcal{X}_q^{u,m,1}$. These search results are used only for calculating the LLR of the $[(u-1)\cdot\log_2(M)+m]$th bit. When the Forward Knowledge Transfer modification is employed, the search results of the DHA related to the $[(u-1)\cdot\log_2(M)+m]$th bit are also used for the calculation of the LLRs of the subsequent bits $b_{[(u-1)\cdot\log_2(M)+m+1]}$, $b_{[(u-1)\cdot\log_2(M)+m+2]}, \ldots, b_{[U\cdot\log_2(M)]}$ of the multi-level symbol, by being stored in their corresponding sets $\mathcal{X}_q^{u,m+1,0}, \mathcal{X}_q^{u,m+1,1}, \ldots, \mathcal{X}_q^{U,\log_2(M),0}, \mathcal{X}_q^{U,\log_2(M),1}$.

[4]Similarly to the Forward Knowledge Transfer modification, when the Forward & Backward Knowledge Transfer modification is employed, the search results of the DHA related to the $[(u-1)\cdot\log_2(M)+m]$th bit of a multi-level QMSDD symbol vector are also used for the calculation of the LLRs of all the bits $b_1, b_2, \ldots, b_{[U\cdot\log_2(M)]}$ of the multi-level symbol, by being stored in their corresponding sets $\mathcal{X}_q^{1,1,0}, \mathcal{X}_q^{1,1,1}, \ldots, \mathcal{X}_q^{U,\log_2(M),0}, \mathcal{X}_q^{U,\log_2(M),1}$.

the sets $\mathcal{X}^{t,m,\mathrm{v}}$. The NE technique is also applicable in the DHA-MUA QMSDD.

Moreover, let us assume that $\mathcal{X}^{t,m,1}$ contains more symbols than $\mathcal{X}^{t,m,0}$, i.e. we have that $\left|\mathcal{X}^{t,m,1}\right| > \left|\mathcal{X}^{t,m,0}\right|$. Then, the sets $\bar{\mathcal{X}}^{t,m,0}$ and $\bar{\mathcal{X}}^{t,m,1}$ are created by trimming the last symbols in $\mathcal{X}^{t,m,1}$ with the lowest CF values, so that the resultant set $\bar{\mathcal{X}}^{t,m,1}$ has the same size as $\bar{\mathcal{X}}^{t,m,0} = \mathcal{X}^{t,m,0}$. Let us also define the sign variable $\varsigma_{t,m}$, which is equal to $+1$ if the globally optimal symbol $\hat{\mathbf{x}}_{\min}$ belongs to $\bar{\mathcal{X}}^{t,m,0}$, otherwise it is -1.

Afterwards, we calculate the difference between the CF values of the respective last symbols in the sorted $\bar{\mathcal{X}}^{t,m,0}$ and $\bar{\mathcal{X}}^{t,m,1}$ sets. If the sign of the result does not match the value of $\varsigma_{t,m}$, both symbols are deleted from their respective sets and we continue this process with the rest of the symbol pairs until we reach the first elements of each set. If the sign of the difference matches the value of $\varsigma_{t,m}$, no action is taken and we proceed with the next symbol pairs. The newly formed sets are described by $\hat{\mathcal{X}}^{t,m,0}$ and $\hat{\mathcal{X}}^{t,m,1}$. By performing this procedure, we ensure that the resultant LLR's polarity is the same as in the MAP MSDD.

The LLR of the tth symbol's mth bit is calculated as in

$$L_{DHA-MUA,apo}\left(b_t^{(m)}\right) = \ln \frac{\sum_{x\in\hat{\mathcal{X}}^{t,m,0}} \exp\left(-f_{MSDD}^{SISO-DHA}(x)\right)}{\sum_{x\in\hat{\mathcal{X}}^{t,m,1}} \exp\left(-f_{MSDD}^{SISO-DHA}(x)\right)}. \quad (81)$$

In this treatise we will only consider the scenario, where the DHA-MUA QMSDDs adopt the NE technique having a total minimum complexity of

$$\mathcal{C}_{DHA-MUA-NE}^{\min} = \left(4.5\sqrt{M_c^{N_w-1}/2} + L_{DHA}^{CD,\min}\right) \cdot \left(1 + \frac{1}{(N_w-1)\cdot \log_2 M_c}\right) + 1. \quad (82)$$

The BER performances of the DHA-MUA QMSDD are illustrated in Fig. 11 for our system scenario associated with $N_w = 7$, where they are compared to the DHA-MAA QMSDD, DHA-MAA-NE QMSDD and the MAP MSDD. In the same figure we have also plotted the BER curves, when different knowledge transfer techniques are exploited. If we allow a single iteration between the MSDDs and the channel decoders, the performance of the DHA-MUA, DHA-MUA-FKT and DHA-MUA-FBKT QMSDDs is near optimal, with those of the DHA-MUA-FBKT and DHA-MUA-FKT QMSDDs being slightly better than that of the DHA-MUA QMSDD and only 0.12 dB away from that of the optimal MAP MSDD, due to their more intelligent knowledge transfer technique. When we calculate the BER at the output of the decoders after two MSDD-DEC iterations, there is a 0.35 dB loss between the DHA-MUA-FBKT QMSDD and the MAP MSDD. The reason for this increased loss when multiple iterations are performed is the specific nature of the approximations that have been adopted for

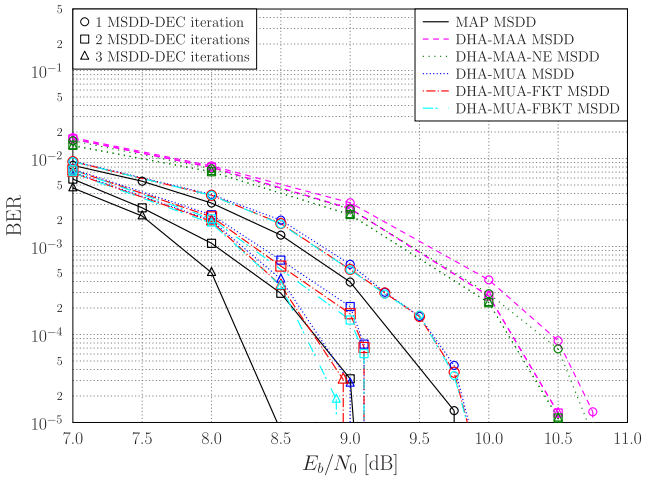

FIGURE 11. BER performance of the family of DHA-MUA QMSDDs and the MAP MSDD in the DSS/SSCH SDMA-OFDM system scenario of Fig. 3, using the parameters summarized in Table 1 for $N_w = 7$.

the QMSDDs, when considering the calculation of the LLRs. During the first MSDD-DEC iteration, the *a priori* LLRs are all-zero, hence they are the same for the MAP MSDD and the QMSDDs. During the second iteration, the *a priori* LLRs of the QMSDDs become different from those of the MAP MSDD, hence eroding the performance. Nonetheless, only 0.1 dB extra transmission power is required for the DHA-MUA-FBKT QMSDD to achieve the same performance as the MAP MSDD. Finally, when $J = 3$ MSDD-DEC iterations are performed, the performance of the QMSDDs becomes similar to their respective performance, when assuming that $J = 2$ MSDD-DEC iterations were allowed, provided that we have $E_b/N_0 < 8$ dB. The power loss between the DHA-MUA-FBKT QMSDD and the MAP MSDD is 0.45 dB at BER $= 10^{-5}$.

The complexities of the QMSDDs are summarized in Table 5 and, once again, the complexities of the QMSDDs

TABLE 5. Complexity in terms of the number of CFEs/bit in Fig. 11.

MSDD / QMSDD	$E_b/N_0 = 8$ dB		
	Number of MSDD-DEC iterations		
	1	2	3
MAP	341.33	341.33	341.33
DHA-MUA	392.17	466.73	501.15
DHA-MUA-FKT	316.72	374.51	401.11
DHA-MUA-FBKT	316.72	374.51	401.11
MSDD / QMSDD	$E_b/N_0 = 4$ dB		
	Number of MSDD-DEC iterations		
	1	2	3
MAP	341.33	341.33	341.33
DHA-MUA	394.06	689.93	962.78
DHA-MUA-FKT	317.87	585.44	820.46
DHA-MUA-FBKT	317.87	585.44	820.46

at multiple MSDD-DEC iterations rely on the E_b/N_0 value. In our scenario we may see that the complexities of the DHA-MUA QMSDDs approach that of the MAP MSDD. Therefore, the family of DHA-MUA QMSDDs is more suitable for non-coherent receivers, where N_w and M are high, for the sake of achieving a higher complexity gain compared to the MAP MSDD, as we will see in Section VII. Since the complexity of the DHA-MUA QMSDD decreases upon increasing the SNR and a typical system is desired to operate around BER $= 10^{-5}$, we expect that the top half of Table 5 will be more applicable in practice. It should also be noted that the complexity of the DHA-MUA QMSDD encountered in our scenario is higher than that of the MAP MSDD even during the first MSDD-DEC iteration, while the complexities of the DHA-MUA-FKT and DHA-MUA-FBKT QMSDDs become higher than that of the MAP MSDD during the second MSDD-DEC iteration. The DHA-MUA-FKT and DHA-MUA-FBKT QMSDDs require more memory than the DHA-MUA, DHA-MAA and DHA-MAA-NE due to the associated knowledge transfer, but their required memory is still smaller than that of the MAP MSDD. Furthermore, the FBKT technique imposes delay on the system, due to the backward knowledge transfer, but once again, the delay is lower than that of the MAP MSDD, where all the bits have to wait for all the CFEs to be performed.

The DHA-MUA QMSDDs are eligible for employment in an iterative receiver, by updating the values of the *a priori* symbol probabilities in (74) and restarting the DHA searches. The inner decoder EXIT curves of the DHA-MUA, DHA-MUA-FKT and DHA-MUA-FBKT QMSDDs in our system scenario of Table 1 are given in Fig. 12 for $E_b/N_0 = 4$ dB and 24 576 bits per frame per user. The inner EXIT curves of the DHA-MUA-FKT and DHA-MUA-FBKT QMSDDs match that of the MAP MSDD, with the inner decoder EXIT curves of the DHA-MUA being a little lower than those of the rest. The fact that the inner decoder EXIT curves of the DHA-MUA-FKT and DHA-MUA-FBKT QMSDDs are slightly higher than that of the MAP MSDD at $I_{MSDD,A} = 0.5$ is due to the simplifications made by the MUA and the visualisation relying on EXIT charts assuming to have Gaussian inputs, similarly to the MAA case. In systems associated with larger search spaces, the difference is expected to be more obvious, since the approximations of the QMSDDs will have a larger impact on the performance.

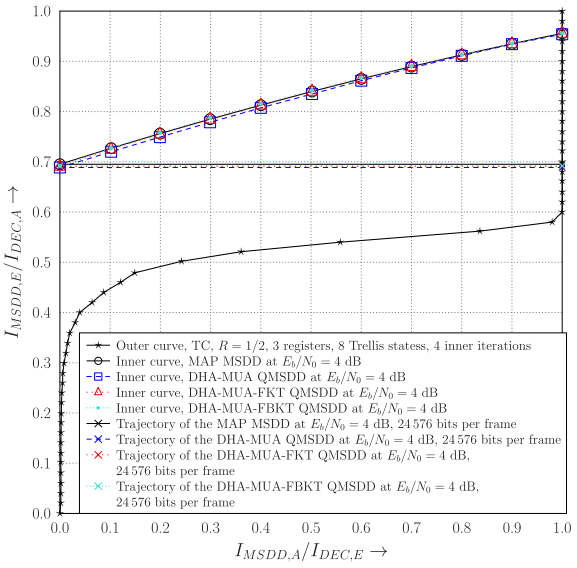

FIGURE 12. EXIT chart of the DHA-MUA, DHA-MUA-FKT and DHA-MUA-FBKT QMSDDs, as well as the MAP MSDD in the DSS/SSCH SDMA-OFDM system scenario of Fig. 3, using the parameters summarized in Table 1 for $N_w = 7$.

E. QUANTUM WEIGHTED SUM ALGORITHM-BASED QMSDD

The QWSA proposed in [14] may be used for performing non-coherent MSDD. The QWSA estimates the weighted sum of a function at a precision, which depends on the number l_{QWSA} of qubits employed in its Quantum Control Register (QCR). The more qubits are used in the QCR, the higher the estimation accuracy becomes, but at the same time, the computational complexity of the QWSA is increased. In our MSDD applications, we use the *a priori* bit-based LLRs of the MSDD, associated with the *a priori* bit probabilities as the weights of the QWSA. At the same time, the function to be estimated by the weighted sum is the normalized CF of the MSDD presented in (51), which leads to:

$$f_{QWSA}(\mathbf{s}) = \frac{\sum_{p=1}^{P} \left(\| \mathbf{U}_p \cdot \mathbf{s} \|_2^2 \right)}{\sum_{p=1}^{P} \left(\| \mathbf{U}_p \cdot \mathbf{s}_{\max} \|_2^2 \right)}, \tag{83}$$

where $\mathbf{s}_{\max}$ is the legitimate multi-level symbol that maximizes the CF of the MSDD in (51). The QWSA only accepts functions that obey $f : \{0, 1, \ldots, N-1\} \rightarrow [0, 1]$. The reason for including the denominator of (83) for normalizing the CF of the QWSA is ensuring that the CF values remains limited to its legitimate value range.

Any search algorithm may be used for finding $\mathbf{s}_{\max}$, which is suitable for calculating the denominator in (83). These are exemplified by the brute force search, ant colony optimization and genetic algorithm-based search. However, suboptimal search methods may output an $\mathbf{s}_{\max}$ value that is different from the true one, in which case the CF value of the true $\mathbf{s}_{\max}$ will have a value higher than 1, hence forcing the QWSA to output erroneous results. In this treatise, the DHA is employed for finding $\mathbf{s}_{\max}$, since we may achieve a $\sim$100% probability of success at a low complexity. The total computational complexity of the DHA-aided QWSA QMSDD expressed in terms of the number of CFEs per bit depends on both the DHA as well as the QWSA and it is in the range of

$$\mathcal{C}_{DHA-QWSA} = 2^{l_{QWSA}+3} + \begin{cases} 22.5\sqrt{M^{N_w-1}} / \left[(N_w - 1) \log_2(M) \right] & \text{upper bound} \\ 4.5\sqrt{M^{N_w-1}} / \left[(N_w - 1) \log_2(M) \right] & \text{lower bound.} \end{cases}$$

According to [14], the DHA-QWSA and hence the DHA-QWSA QMSDD may also be employed in large-scale systems, since its effect can only be evident there. However, we will focus our attention on small-scale systems, due to the practical constraints in our simulation time and memory requirements. Let us employ the DHA-QWSA QMSDD in our system scenario described in Table 1. The BER performance of the DHA-QWSA QMSDD for $l_{QWSA} = 9, 10, 11$ qubits is compared to that of the optimal classical MAP MSDD in Fig. 13. We may verify that by increasing the number of control qubits l_{QWSA} in the QWSA, we improve the system's performance, at the cost of increasing the complexity required to achieve it. For $l_{QWSA} = 10$ qubits, we may achieve a loss of 0.5 dB, when compared to the MAP MSDD, while if $l_{QWSA} = 11$ qubits are used in the QCR of the QWSA, we have a 0.22 dB loss, when $J = 3$ MSDD-DEC iterations are affordable. The total number of CFEs of the DHA-QWSA QMSDDs in Fig. 13 are given in Table 6. Since the complexity of the DHA-QWSA QMSDD is higher than that of the MAP MSDD in every instance of our scenario, it is worth noting once again that the DHA-QWSA QMSDD is suitable for large-scale systems, as are most of the quantum detectors advocated in this treatise. Based on Table 6 we may observe that the performance of the DHA-QWSA QMSDD is almost independent of the power during the first MSDD-DEC iteration, since the number of CFEs per bit is similar for both $E_b/N_0 = 4$ dB and $E_b/N_0 = 8$ dB. On the other hand, when we can afford multiple MSDD-DEC iterations, the complexity becomes lower, when the power is increased, which is due to the fact that a second or a third MSDD-DEC iteration is required less often, because the frame is perfectly decoded during the first or second MSDD-DEC iteration.

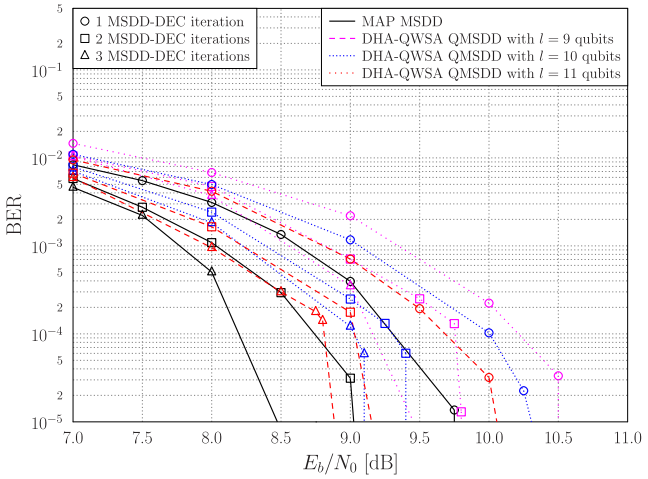

FIGURE 13. BER performance of the DHA-aided QWSA QMSDD and the MAP MSDD in the DSS/SSCH SDMA-OFDM system scenario of Fig. 3, using the parameters summarized in Table 1 for $N_W = 7$, when using $l_{QWSA} = 9, 10, 11$ control qubits in the QWSA.

Fig. 14 presents the EXIT chart of our scenario for a single frame transmitted by each user at $E_b/N_0 = 4$ dB.

TABLE 6. Complexity in terms of the number of CFEs/bit in Fig. 13.

MSDD / QMSDD		$E_b/N_0 = 8$ dB		
		Number of MSDD-DEC iterations		
		1	2	3
MAP		341.33	341.33	341.33
QWSA	$l_{QWSA} = 9$	4139.65	5266.92	6004.28
	$l_{QWSA} = 10$	8235.71	10 100.34	10 919.02
	$l_{QWSA} = 11$	16 427.67	19 849.57	21 323.38
MSDD / QMSDD		$E_b/N_0 = 4$ dB		
		Number of MSDD-DEC iterations		
		1	2	3
MAP		341.33	341.33	341.33
QWSA	$l_{QWSA} = 9$	4139.66	8235.68	12 331.66
	$l_{QWSA} = 10$	8235.80	16 427.73	24 619.80
	$l_{QWSA} = 11$	16 427.80	32 811.80	49 195.80

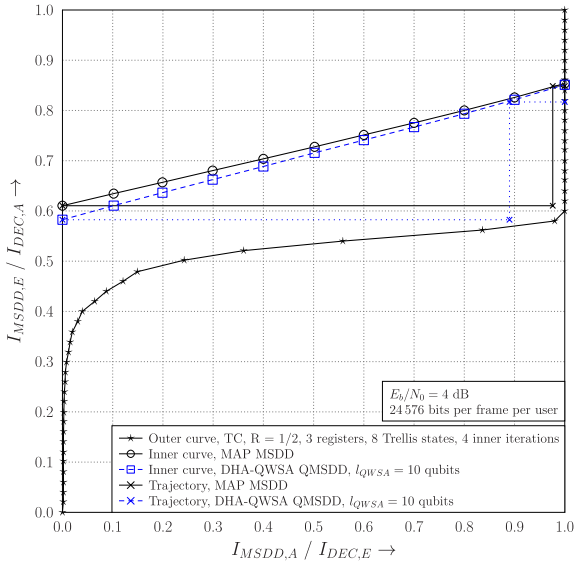

FIGURE 14. EXIT chart of the QWSA QMSDD with $l_{QWSA} = 10$ qubits, as well as the MAP MSDD in the DSS/SSCH SDMA-OFDM system scenario of Fig. 3, using the parameters summarized in Table 1 for $N_W = 7$.

According to Fig. 14, the frame length of 24 576 bits per frame per user was not sufficient for the specific Monte-Carlo decoding trajectory to be fully decoded by the MAP MSDD after one iteration. Both the MAP MSDD and the DHA-QWSA QMSDD successfully reach the $I_{DEC,E} = 1$ point after two MSDD-DEC iterations. By observing Fig. 14 we may conclude that the DHA-aided QWSA QMSDD may be beneficially incorporated into an iterative receiver, since its inner decoder EXIT curve matches that of the MAP MSDD.

V. EXPLOITATION OF THE CONVENTIONAL DIFFERENTIAL DETECTOR

All the MSDDs that detect the transmitted symbols over an N_w-long symbol window require the reception of N_w signals.

In our discussions presented in the previous sections, we have assumed having a random initial input to the DHA, since we have no *a priori* information about the transmitted multi-level symbol. When we used coherent multi-user detection in [12] and [13], we initialized the DHA searches with the output symbol of either the MF, ZF or the MMSE detectors.

By assuming that the signals arrive in the same sequence as they were transmitted, we may be able to perform CDD for every consecutively formed received signal pair in each N_w-long symbol window, while waiting for all the N_w signals to be received. Once all the signals are received and the QMSDD procedure can be initiated, the combined outputs of the $(N_w - 1)$ CDDs may be used as the initial input of the corresponding DHA search. Therefore, no additional delay is imposed on the QMSDD and there is only a modest increase in complexity, since the $(N_w - 1)$-fold increase of the CDD applications is compensated by the lower complexity required by a deterministically-initialized DHA. By exploiting the CDD in our scenario described in Table 1, the resultant procedure is described in Fig. 15, where the first detection window is presented.

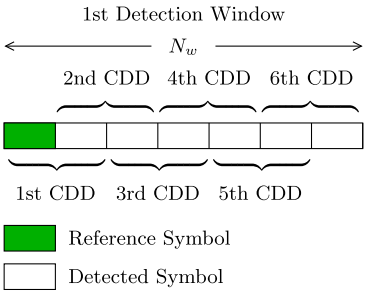

FIGURE 15. Exploitation of the CDD for initializing the DHA searches in the first detection window of the QMSDDs, resulting in reduced complexity and same performance.

More specifically, we firstly receive the reference signal, which is buffered. When the second signal is received, we perform the CDD on the first two received signals, obtaining the symbol index output $x_{CDD,1} \in \{0, 1, \ldots, M-1\}$. Both received signals remain buffered. After the third signal has arrived, the CDD is applied for the detection window formed by the second and third signal, where the second signal acts as the reference, which is equal to $x_{CDD,1}$. The output of the second CDD is $x_{CDD,2} \in \{0, 1, \ldots, M-1\}$. The same process is repeated, until all N_w signals have been received and $(N_w - 1)$ CDDs have been performed, obtaining $x_{CDD,k}$, $k = 1, 2, \ldots, N_w - 1$. Finally, we are ready to combine the CDD outputs for the sake of obtaining a multi-level symbol index, which may be the initial symbol of the DHA in the QMSDD employed. The initial multi-level symbol index is equal to

$$x_{init} = \sum_{k=1}^{N_w-1} x_{CDD,k} \cdot M^{N_w-1-k}. \tag{84}$$

During the second detection window, the procedure ensues similarly to the one analysed during the first detection window, with the slight difference that instead of a reference symbol, the output of the QMSDD generated for the last symbol of the previous detection window is used. The visual representation of the CDD activation for the nth detection window is depicted in Fig. 16. By using the CDD initialization, we essentially perform a CDD for every unknown symbol. Therefore, the additional complexity of the CDD initialization imposed to the overall detection complexity in terms of number of CFEs per bit is equal to

$$\mathcal{C}_{CDD,init} = \frac{M}{\log_2(M)}. \tag{85}$$

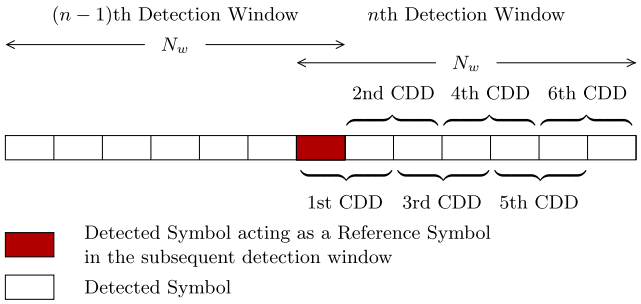

FIGURE 16. Exploitation of the CDD for initializing the DHA searches in the *n*th detection window of the QMSDDs, resulting in reduced complexity and same performance.

A. HARD-OUTPUT CDD-INITIALIZED QMSDD

The impact of the deterministic CDD initialization of the DHA is more apparent, when we use the DHA QMSDD of Section IV-A. Fig. 17 shows the PDF and CDF curves of our system scenario presented in Table 1, when we either initialize the DHA using the CDD outputs or randomly. In the same figure, we may observe that the DHA finds the solution sooner, when it is initialized by the CDD instead of being randomly initialized. This is indeed expected, since the closer we start the search to the optimal symbol, the faster the optimal symbol will be found and the search will be concluded. It is reasonable to expect that the DHA search is completed sooner when the initial symbol is the optimal one. Based on the CDF curves seen in Fig. 7 we may also invoke the "CDD-initialized" ES-DHA for achieving a near-optimal performance at an even lower complexity. For example, if we stop the CDD-initialized ES-DHA QMSDD of Fig. 7 in Section IV-B after $363 - 313 = 50$ CFEs, we will have found the optimal multi-level symbol with a success probability of 90%, where in our scenario 313 is the minimum number of CFEs that the DHA needs for realizing that the solution has indeed been found in our scenario. On the other hand, we will require $656 - 313 = 343$ CFEs to achieve the same probability of success with a randomly-initialized ES-DHA QMSDD. It is reasonable to conclude that achieving a good performance by the CDD is vital for the sake of attaining a substantial complexity reduction by the CDD-initialized DHA QMSDD. According to Fig. 6, the BER performance of the CDD was 0.5 dB away from that of the ML MSDD,

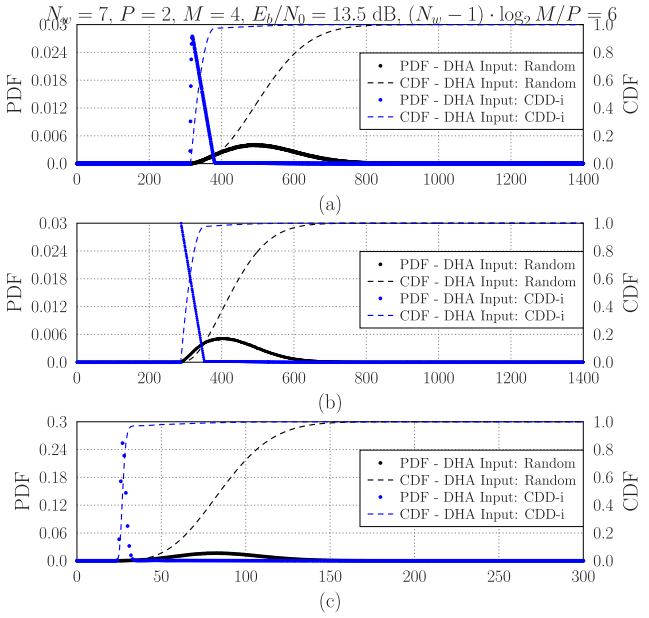

FIGURE 17. PDF and CDF curves of the DHA in the scenario of Fig. 3, using the parameters summarized in Table 1 for $N_w = 7$ after $12 \cdot 10^6$ number of independent DHA instances, when the DHA searches are initialized by using the pre-calculated CDD outputs or by using a random symbol index. (a) Total number of CF evaluations. (b) Number of Grover iterations (CF evaluations in the QD). (c) Number of CF evaluations in the CD.

therefore its outputs were identical to the optimal symbol most of the time, as it can also be inferred from the shape of the CDD-initialized DHA QMSDD's PDF curve portrayed in Fig. 17a. The BER performance of the CDD-initialized DHA QMSDD is expected to be equivalent to that of the randomly-initialized DHA QMSDD. This is indeed verified in Fig. 18, where we may observe that the CDD-initialized DHA QMSDD performs equivalently both to the random-initialized DHA QMSDD and to the ML MSDD.

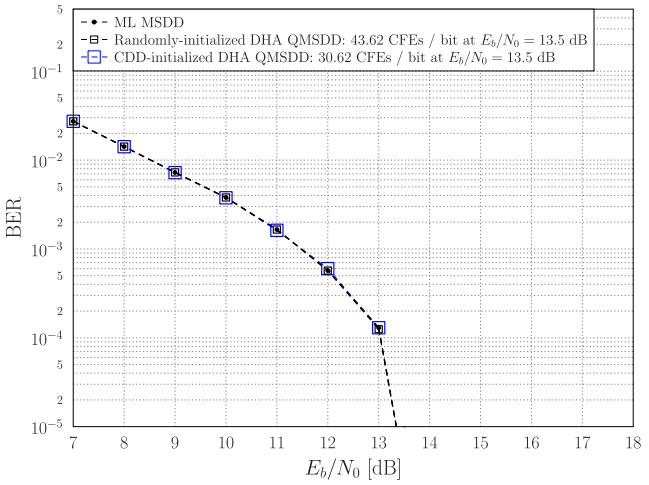

FIGURE 18. BER performance of the randomly-initialized and CDD-initialized DHA QMSDD in the DSS/SSCH SDMA-OFDM system scenario of Fig. 3, using the parameters summarized in Table 1 for $N_w = 7$.

B. SOFT-INPUT SOFT-OUTPUT CDD-INITIALIZED QMSDD

The initialization of the DHA searches with the aid of the CDD outputs may also be used in the SISO DHA-aided QMSDDs of Fig. 11 in Section IV-D. The effect of the CDD-aided initialization of the DHA search in the SISO QMSDDs is not as straightforward as in the hard-output QMSDDs, since the goal is not only to find the optimal multi-level symbol, but also to create a set of the best symbols found. By commencing the search closer to the optimal multi-level symbol, we may exclude a number of near-optimal symbols that would have been found, if the randomly-initialized search was used instead.

In addition to the CDD-aided initialization of the DHA searches, in the iterative QMSDDs we may also use the optimal multi-level symbol found during the first MSDD-DEC iteration as the initial input of the DHA search during the second MSDD-DEC iteration. Similarly, the best symbol found during the second MSDD-DEC iteration may initialize the DHA search of the same detection window during the third MSDD-DEC iteration and so on. In this way, the CDD is performed only during the first MSDD-DEC iteration and no additional complexity is imposed by initializing the DHA search during the subsequent MSDD-DEC iterations. Let us use the term *deterministic initialization* in the context of the SISO QMSDD, when we employ the CDD-based initialization for the DHA searches during the first QMSDD-DEC iteration and we use the best found symbols for initializing the DHA searches of the subsequent QMSDD-DEC iterations.

The BER performance of the deterministically-initialized DHA-MUA-FKT QMSDD is compared in Fig. 19 both to that of the randomly-initialized DHA-MUA-FKT QMSDD

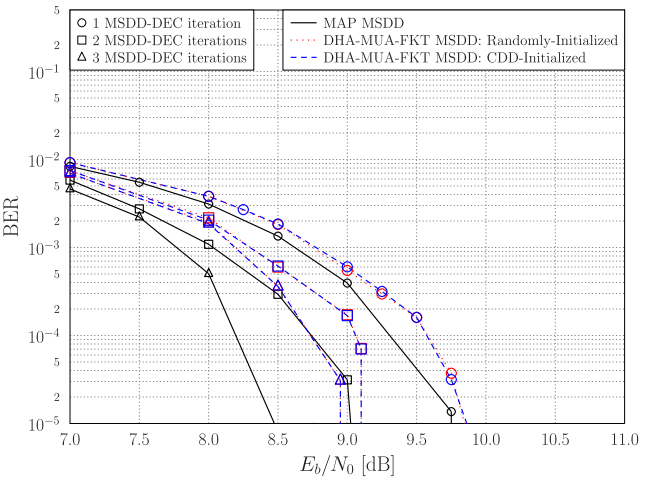

FIGURE 19. BER performance of the CDD-initialized and randomly-initialized DHA-MUA-FKT QMSDD in the DSS/SSCH SDMA-OFDM system scenario of Fig. 3, using the parameters summarized in Table 1 for $N_w 7 = 7$. The CDD-initialized DHA-MUA-FKT QMSDD also employs deterministic DHA initialization during the second and third MSDD-DEC iterations by using the optimal symbol of each detection window found during the previous MSDD-DEC iteration.

TABLE 7. Complexity in terms of the number of CFEs/bit in Fig. 19.

MSDD / QMSDD	$E_b/N_0 = 8$ dB		
	Number of MSDD-DEC iterations		
	1	2	3
MAP	341.33	341.33	341.33
DHA-MUA-FKT			
Random Initialization	316.72	374.51	401.11
Deterministic Initialization	317.74	374.11	399.94
Random Initialization & Iteration memory	316.72	373.07	398.86
DHA-MUA			
Random Initialization	392.17	466.73	501.15
Deterministic Initialization	384.29	455.13	487.74
MSDD / QMSDD	$E_b/N_0 = 4$ dB		
	Number of MSDD-DEC iterations		
	1	2	3
MAP	341.33	341.33	341.33
DHA-MUA-FKT			
Random Initialization	317.87	585.44	820.46
Determinstic Initialization	318.75	581.18	810.12
Random Initialization & Iteration memory	317.87	580.30	809.16
DHA-MUA			
Random Initialization	394.06	689.93	962.78
Deterministic Initialization	387.25	673.33	926.09

of Fig. 11 as well as to that of the MAP MSDD of Fig. 11, while their respective computational complexities are given in Table 7. Based on Fig. 19, the performance of the CDD-initialized DHA-MUA-FKT QMSDD is seen to be equivalent to that of the randomly-initialized DHA-MUA-FKT QMSDD. According to Table 7, the complexity of the deterministically-initialized DHA-MUA-FKT QMSDD is higher than that of the randomly-initialized DHA-MUA-FKT QMSDD during the first QMSDD-DEC iteration and it becomes lower during the second and third QMSDD-DEC iteration. The reason that the deterministically-initialized DHA-MUA-FKT QMSDD of Fig. 19 has a higher complexity lies in its nature, where multiple DHA searches take place. For example, let us focus our attention on the nth detection window. The two DHA searches of the multi-level symbol's first bit will be concluded sooner in the deterministically-initialized DHA-MUA-FKT QMSDD than in the randomly-initialized DHA-MUA-FKT QMSDD, as it was also shown in the case of the hard-output DHA QMSDD of Section V-A. Therefore, it is expected for the resultant sets $\mathcal{X}^{1,1,0}$ and $\mathcal{X}^{1,1,1}$ of the deterministically-initialized DHA-MUA-FKT QMSDD to contain fewer elements. According to the methodology followed by the DHA-MUA-FKT QMSDD, the subsequent DHA searches of the rest of the bits in the multi-level symbols are initialized either based on the best already found symbols during the previous DHA searches due to the forward knowledge transfer, or based on the neighbours of the globally optimal symbol. Therefore, the more elements are included in the sets $\mathcal{X}^{1,1,0}$ and $\mathcal{X}^{1,1,1}$, the higher the probability of initializing the DHA search of the second bit closer to its optimal symbol. Hence, the randomly-initialized DHA-MUA-FKT QMSDD has the edge over the deterministically-initialized DHA-MUA-FKT QMSDD during this part due to the size of its initial sets $\mathcal{X}^{1,1,0}$ and $\mathcal{X}^{1,1,1}$, effectively mitigating the complexity imposed during the first bit's first DHA search. After the DHA searches of the first few bits have been completed, the deterministically-initialized DHA-MUA-FKT QMSDD of Fig. 19 has also increased its sets' size and the complexity of the DHA searches conducted for the rest of the bits in the multi-level symbol is similar to that in its randomly-initialized counterpart. It should be noted that in the DHA-MUA QMSDD, where there is no knowledge transfer, the deterministically-initialized DHA-MUA QMSDD will have a lower complexity than its randomly-initialized counterpart, as portrayed in Table 7.

During the subsequent QMSDD-DEC iterations, the initial advantage of the deterministically initialized DHA-MUA-FKT QMSDD of Fig. 19 becomes more dominant, since the initialization of the first bit's first DHA is the best found symbol during the previous QMSDD-DEC iteration and it often remains the optimal symbol of the specific detection window during the rest of the QMSDD-DEC iterations. This results in the deterministically-initialized DHA-MUA-FKT QMSDD essentially initializing the first bit's DHA search with its solution. The deterministically-initialized DHA-MUA-FKT is expected to have fewer elements in the $\mathcal{X}_q^{t,m,\mathrm{v}}$ sets than its randomly-initialized counterpart, since it will reach the optimal multi-level MSDD symbol vector after fewer CFEs, which in turn leads to fewer unique CF values found. The problem of the smaller set size arrived at after the first two DHA searches also persists for the deterministically-initialized DHA-MUA-FKT QMSDD, but the difference in complexity reduction is not mitigated sufficiently rapidly by the randomly-initialized DHA-MUA-FKT QMSDD of Fig. 19.

In Table 7 we also characterize the randomly-initialized DHA-MUA-FKT QMSDD with iteration memory, which uses a randomly selected initial input for the DHA searches during the first MSDD-DEC iteration and then later employs the globally optimal multi-level symbol found during the previous iteration for the subsequent MSDD-DEC iterations. The randomly-initialized DHA-MUA-FKT QMSDD associated with an iteration memory uses a random initial input only during the $J = 1$st MSDD-DEC iteration. For the subsequent $J \geq 2$ MSDD-DEC iterations the best symbol found during the previous MSDD-DEC iteration is used instead for the sake of initializing the DHA. This hybrid semi-deterministically-initialized DHA-MUA-FKT QMSDD has a complexity, which is identical to that of

the randomly-initialized DHA-MUA-FKT QMSDD during the first iteration, while its complexity during the rest of the iterations is similar to that of ts deterministically-initialized counterpart.

VI. EMPLOYMENT OF THE QMSDD ONLY AFTER EVERY *IpS* QMSDD-DEC ITERATIONS

In case of coherent detection, when we use the MAP MUD we may assume that improved channel estimates become available during the subsequent MUD-DEC iterations, therefore the MAP MUD should re-evaluate the CF for all the legitimate multi-level symbols during each MUD-DEC iteration, which, inevitably increases its complexity upon each additional iteration. By contrast, in case of non-coherent detection, the MAP MSDD is only employed during the first MSDD-DEC iteration and the hitherto computed complete set of CFEs is reused during the subsequent MSDD-DEC iterations. In this treatise, we assume that the reuse of the same hitherto found CFE set is granted without any additional computational complexity, since our metric is selected to be the number of CFEs performed by an MSDD. This may have been observed in Table 4, Table 5, Table 6 and Table 7, where the complexity of the MAP MSDD remains constant over the three MSDD-DEC iterations.

However, we have employed our QMSDDs during each QMSDD-DEC iteration, taking into consideration the fact that there is a possibility that during the second QMSDD-DEC iteration the globally optimal symbol may be a symbol that was not found during the first QMSDD-DEC iteration. This may occur, since the proposed QMSDDs find a suitable subset of symbols used for calculating the bit-based LLRs, instead of calculating the CFE corresponding to every legitimate multi-level symbol, as in the MAP MSDD.

In this section we investigate the effect of actively not employing the DHA-MUA-FBKT QMSDD during every QMSDD-DEC iteration in our scenario presented in Table 1 in the interest of reducing the complexity imposed. During the specific QMSDD-DEC iterations which dispense with employing the QMSDD, the LLRs are calculated based on the most recently found CFE set and the newly obtained *a priori* probabilities gleaned from the channel decoder. Hence, the CF that is used when the QMSDD is employed does not include the *a priori* probabilities, which is in contrast to (75) and it becomes

$$f_{MSDD,IpS}^{SISO-DHA}(\mathbf{x}) = \sum_{p=1}^{P} \left(\| \mathbf{U}_p \cdot \mathbf{s} \|_2^2 \right), \tag{86}$$

where the relationship between $\mathbf{s}$ and $\mathbf{x}$ is described in (1). By dispensing with the employment of the QMSDD during each QMSDD-DEC iteration and by exploiting both the previously found symbol as well as the CFE sets we expect an even lower complexity, albeit at the cost of a BER performance degradation. It should be noted that the entire CFE set that was found during the most recent QMSDD-DEC iteration, where the QMSDD was used will be exploited for the calculation of the LLRs during the QMSDD-DEC iterations, where the QSMDD is not used, by substituting the CF values in (55), along with the updated *a priori* probabilities.

Fig. 20 presents the BER performance of the randomly-initialized DHA-MUA-FBKT QMSDD of Section IV-D relying on having an iteration memory in our scenario as portrayed in Section V-B, when it is employed during every QMSDD-DEC iteration. In other words, this corresponds to an Iterations per Search (*IpS*) ratio of $IpS = 1$. Furthermore, the scenarios of $IpS = 2, 3$ and 6 are also presented in Fig. 20. We may observe that the BER performance is worse, when we employ the QMSDD less frequently. However, the complexity reduction attained by reusing the same, previously obtained sets diminishes upon increasing the number of QMSDD-DEC iterations. Observe in Fig. 20 that there is a trade-off between the performance gain and the decoding complexity obtained by a QMSDD-DEC iteration, where the previously found symbol set is used.

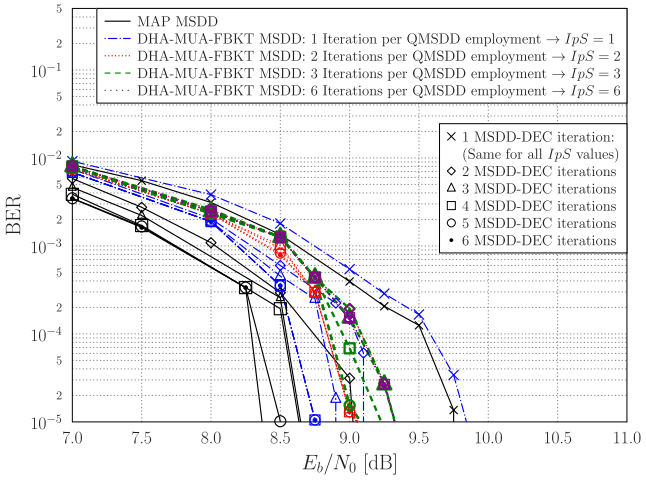

FIGURE 20. BER performance of the randomly-initialized DHA-MUA-FBKT QMSDD with iteration memory in the DSS/SSCH SDMA-OFDM system described in Fig. 3, using the parameters summarized in Table 1 for $N_w = 7$ and $IpS \in \{1, 2, 3, 6\}$.

Based on Fig. 20 we observe that as expected, the gain achieved during an additional iteration, when the QMSDD is employed is higher than that when the previously obtained CFE set is used. However, the performance degradation may not be severe, whilst the attainable complexity reduction is substantial. For example, the performance of the DHA-MUA-FBKT QMSDD associated with $IpS = 3$ after $J = 3$ MSDD-DEC iterations is 0.25 dB away from that of its counterpart relying on $IpS = 1$ at BER $= 10^{-5}$. In other words, in this scenario if we employ the DHA-MUA-FBKT QMSDD only during the first MSDD-DEC iteration, similarly to the MAP MSDD, we would need 0.25 dB more power for achieving the same performance as in the case, where we employed $J = 3$ MSDD-DEC iterations. The complexities of the systems investigated are summarized in Table 8. It should be noted

TABLE 8. Complexity in terms of the number of CFEs/bit in Fig. 19.

MSDD / QMSDD	$E_b/N_0 = 8$ dB		
	Number of MSDD-DEC iterations		
	1	2	3
MAP	341.33	341.33	341.33
DHA-MUA-FBKT			
$IpS = 1$	316.72	374.51	401.11
$IpS = 2$	316.72	316.72	346.97
$IpS = 3$	316.72	316.72	316.72
$IpS = 6$	316.72	316.72	316.72
MSDD / QMSDD	Number of MSDD-DEC iterations		
	4	5	6
MAP	341.33	341.33	341.33
DHA-MUA-FBKT			
$IpS = 1$	412.99	426.07	439.15
$IpS = 2$	346.97	368.65	368.65
$IpS = 3$	342.73	342.73	342.73
$IpS = 6$	316.72	316.72	316.72

that similarly to the MAP MSDD, the complexity of the QMSDD relying on the previously found sets being reused remains the same.

VII. EFFECT OF THE DETECTION WINDOW LENGTH AND THE FREQUENCY OF SUBCARRIER HOPPING

In non-coherent multiple-symbol differential detection, extending the length of the detection window N_w has a beneficial impact on the system's performance, which however has to be traded-off against the detector's complexity. Explicitly, the MAP MSDD's complexity increases exponentially with the detection window's size, but the BER performance is improved. This is illustrated in Fig. 21, where we investigate the system specified in Table 1 with the slight difference that 10 752 bits are transmitted by each of the 4 users in each frame, when we have $N_w = 8$ and $N_w = 4$ and when QPSK modulation associated with $M = 4$ is used, resulting in a search space of $M^{N_w-1} = 16\,384$ and 64 legitimate multi-level symbols, respectively. We may observe that fewer bit errors occur at the end of the channel decoding procedure, for $N_w = 8$ than in the case of $N_w = 4$ for the same E_b/N_0 value. More specifically, the performance gap between the $N_w = 8$ system and the $N_w = 4$ system is approximately 0.3 dB, when a single MSDD-DEC iteration is performed and 0.5 dB when we allow 2 or 3 MSDD-DEC iterations. However, the complexity of the $N_w = 8$ MAP MSDD quantified in terms of the number of CFEs per bit is 109.68 times higher than that of the MAP MSDD, which uses $N_w = 4$. In more detail, according to (60), the complexity of the MAP MSDD associated with $N_w = 8$ is equal to 1170.3 CFEs per bit, while only 10.67 CFEs per bit are required by the MAP MSDD for $N_w = 4$.

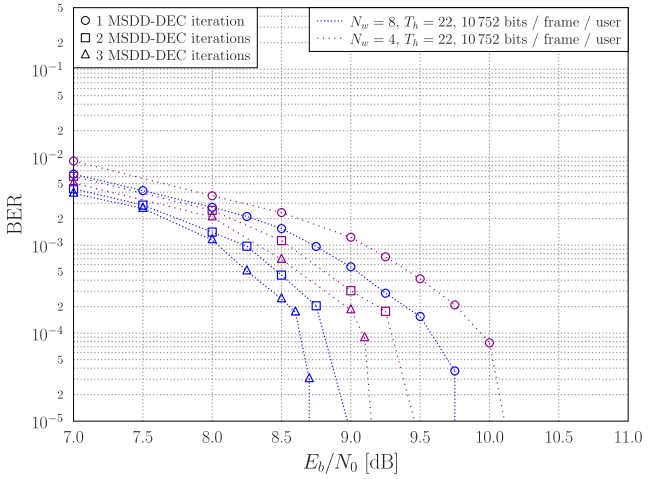

FIGURE 21. BER performance of the MAP MSDD in the DSS/SSCH SDMA-OFDM system described in Fig. 3, using the parameters summarized in Table 1 for 10 752 bits per frame per user and $N_w \in \{4, 8\}$.

It should be noted that in both systems characterized in Fig. 21 the same value was used for the period of subcarrier hopping T_h. The reason T_h was kept the same is that of providing a fair comparison between the MSDDs having different detection window lengths. In fact, even by keeping the value of T_h the same, there is a difference in the operation of the MAP MSDDs using $N_w = 8$ and $N_w = 4$, since the former one has to detect the signal of $(T_h - 1)/(N_w - 1) = 21/7 = 3$ windows after the most recent reception of a reference symbol and before a new reference symbol arrives on a different subcarrier, while the MAP MSDD associated with $N_w = 4$ has to detect the signals gleaned from $(T_h - 1)/(N_w - 1) = 21/3 = 7$ windows during the same period. Naturally, the difference in the number of detection windows affects the system's performance in the case, where the last symbol of a detection window which is subsequently used as the reference symbol of the next detection window has been erroneously detected. That scenario occurs more frequently, when we have a shorter window length N_w and a longer subcarrier hopping period T_h.

When we increase the subcarrier hopping period T_h, we require the transmission of fewer reference symbols, since each user transmits on the same slow-fading subcarrier for a longer period of time, therefore increasing the system's throughput. At the same time however, we do not allocate the resources to the users in a fair manner, since in the scenario of a user operating in a deeply-fading channel, that user will have to continue to have to suffer for the duration of T_h symbols. A trade-off between the throughput and quality of service has to be struck in the SSCH multi-carrier systems.

In our QMSDD application, the value of T_h may have an additional impact in the performance of the system. Explicitly, when we increase the subcarrier hopping period T_h, the number of consecutive detection windows with only the first symbol of the first detection window of that chain being a reference symbol is also increased. Intuitively, this would lead to a worse BER performance

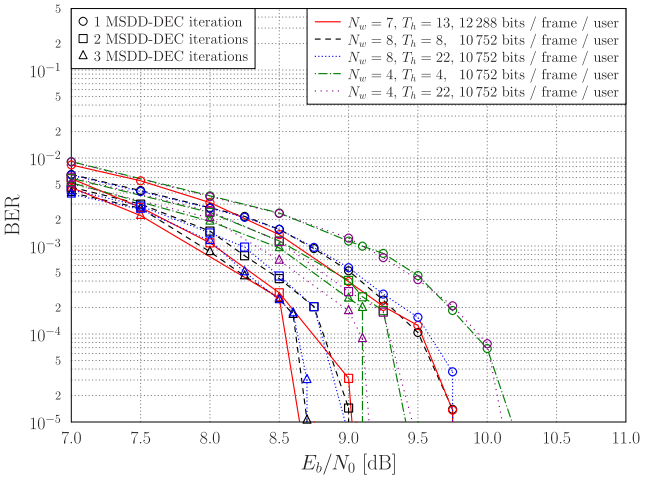

FIGURE 22. BER performance of the MAP MSDD in the DSS/SSCH SDMA-OFDM system described in Fig. 3, using the parameters summarized in Table 1 for 10 752 bits per frame per user and $[N_w, T_h] \in \{[8, 8], [8, 22], [4, 4], [4, 22]\}$.

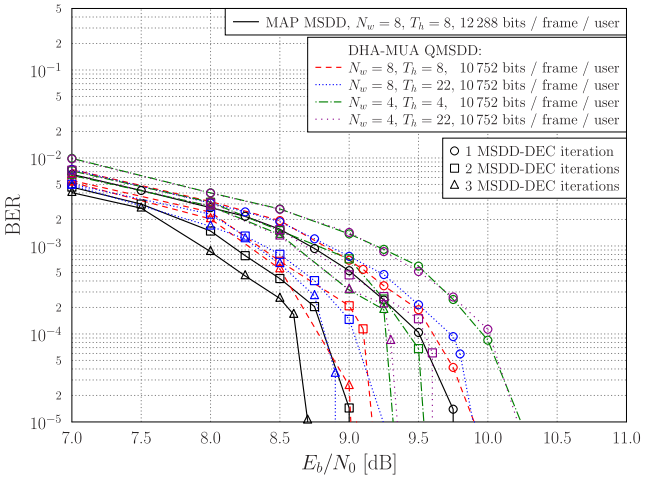

FIGURE 23. BER performance of the deterministically-initialized DHA-MUA QMSDD with iteration memory in the DSS/SSCH SDMA-OFDM system of Fig. 3, using the parameters summarized in Table 1 for 10 752 bits per frame per user and $[N_w, T_h] \in \{[8, 8], [8, 22], [4, 4], [4, 22]\}$.

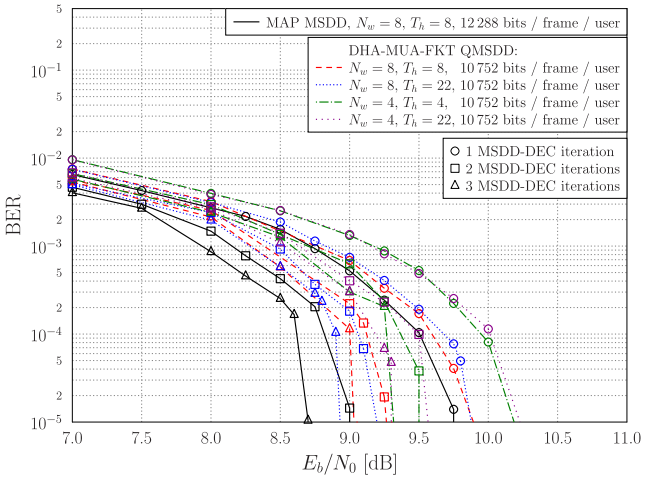

FIGURE 24. BER performance of the deterministically-initialized DHA-MUA-FKT QMSDD with iteration memory in the DSS/SSCH SDMA-OFDM system of Fig. 3, using the parameters summarized in Table 1 for 10 752 bits per frame per user and $[N_w, T_h] \in \{[8, 8], [8, 22], [4, 4], [4, 22]\}$.

than when the subcarrier hopping period T_h is equal to the detection window's length N_w and hence a reference symbol is transmitted for each detection window. In Fig. 22, we show the BER performance of our system, when we use the MAP MSDD associated with $[N_w, T_h] \in \{[8, 8], [8, 22], [4, 4], [4, 22]\}$. We may conclude that the value of T_h has an impact on the BER performance, even though the gain achieved is relatively modest and should be considered in the light of the associated system throughput reduction. Interestingly, in the case of $N_w = 4$, the performance improves, when we increase T_h in the BER $= 10^{-2} - 10^{-4}$ range, but when operating at BER $= 10^{-5}$, the performance of the two MAP MSDDs remains essentially the same.

For comparison, in Fig. 22 we have also included the BER curves of the MAP MSDD associated with $[N_w = 7, T_h = 13]$, where each user transmits 12 288 bits per frame. The objective of this comparison is that of determining the impact of the detection window's length N_w, when contrasted to an increased interleaver length and hence a commensurately improved channel decoding performance. Based on Fig. 22, the BER performance of the MAP MSDD using $[N_w = 8, T_h = 8]$ when 10 752 bits per frame per user are transmitted is equivalent to that of the MAP MSDD associated with $[N_w = 7, T_h = 13]$ when 12 288 bits per frame per user are used. Therefore, the interleavers' length and the value of the detection window's length N_w have the most substantial impact on a system, while that of the subcarrier hopping period T_h is significantly lower.

In Fig. 23, Fig. 24 and Fig. 25 we present the BER performance with respect to the E_b/N_0 values of the deterministically-initialized DHA-MUA QMSDD, DHA-MUA-FKT QMSDD and DHA-MUA-FBKT QMSDD, respectively, all equipped with an iteration memory for the sake of updating the initial guess of the DHA searches. In the same figures, we have replotted the BER performance of the MAP MSDD associated with $[N_w = 8, T_h = 8]$ for comparison. As expected, the QMSDDs using $[N_w = 8, T_h = 8]$ performs close to the optimal MAP MSDD. Once again, the effect of T_h is not very pronounced, since systems having the same detection window length N_w perform equally well. On the other hand, by increasing N_w we achieve an improved BER performance at the cost of a concomitant increase in complexity, as stated in Table 9, where only the complexities of the QMSDDs that employ $N_w = 8$ are stated, since their complexity recorded for $N_w = 4$ is higher than that of the respective MAP MSDD associated with $N_w = 4$. It should be noted that the value of T_h does not affect the complexity of the QMSDD, therefore the same QMSDDs that employ $[N_w = 8, T_h = 8]$ and $[N_w = 8, T_h = 22]$ have an identical complexity

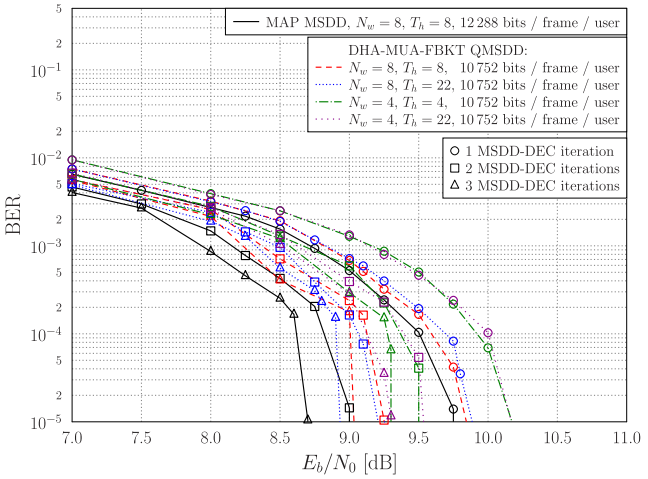

FIGURE 25. BER performance of the deterministically-initialized DHA-MUA-FBKT QMSDD with iteration memory in the DSS/SSCH SDMA-OFDM system of Fig. 3, using the parameters summarized in Table 1 for 10 752 bits per frame per user and $[N_w, T_h] \in \{[8, 8], [8, 22], [4, 4], [4, 22]\}$.

TABLE 9. Complexity in terms of the number of CFEs/bit of the QMSDDs that use $N_w = 8$ in Fig. 22, Fig. 23, Fig. 24 and Fig. 25.

MSDD / QMSDD	$E_b/N_0 = 9$ dB		
	Number of MSDD-DEC iterations		
	1	2	3
MAP	1170.30	1170.30	1170.30
DHA-MUA	739.82	775.47	781.79
DHA-MUA-FKT	604.95	639.17	645.11
DHA-MUA-FBKT	604.95	639.17	645.11

in terms of the CFEs. Based on Table 9, the QMSDDs have lower complexities than the MAP MSDD, even after $J = 3$ MSDD-DEC iterations. A comparison between the complexities stated in Table 5 and Table 9, which characterize the same QMSDDs associated with $N_w = 7$ and $N_w = 8$, respectively, demonstrates the scaling of the QMSDDs' complexities with respect to that of the MAP MSDD. The reason for the associated slight increase of the number of CFEs per bit required in the QMSDDs when adding an extra QMSDD-DEC iteration is that due to the relatively high value of $E_b/N_0 = 9$ dB, most of the frames were successfully decoded during the previous iterations. Therefore, only the erroneously detected frames will participate in the subsequent MSDD-DEC iteration. When the value of E_b/N_0 is lower, the complexity of the QMSDDs seen in Table 9 becomes higher, while that of the MAP MSDD will remain the same. However, since typically it is required for the systems to operate at BER $= 10^{-5}$ or even lower, the choice of $E_b/N_0 = 9$ dB satisfies the QMSDDs associated with $J = 3$ QMSDD-DEC iterations.

VIII. CONCLUSIONS

In this treatise we answered a number of design dilemmas. More explicitly, we argued in favour of the family of non-coherent receivers, which do not require channel estimates, in contrast to their higher-complexity coherent receiver counterparts, which rely on the accuracy of the channel estimation. Therefore, the complexity of the non-coherent receivers is lower, but their BER performance is degraded, when compared to that of a coherent receiver provided with perfect channel estimates. Furthermore, we showed that the MSDD performs better than the CDD, by performing detection over an extended window of several symbols. Based on the complexity reduction achieved by the quantum algorithms over their classical counterparts, we opted for exploiting them in the context of MSDD in non-coherent receivers, whilst achieving a near-optimal performance at a reduced complexity.

We introduced a number of quantum-assisted multi-symbol differential detectors. More specifically, we investigated the HIHO DHA QMSDD and ES-DHA QMSDD in Section IV-A and Section IV-B, respectively, as well as the SO DHA-MAA QMSDD and DHA-MAA-NE QMSDD in Section IV-C. Furthermore, we presented the SISO DHA-MUA QMSDD, DHA-MUA-FKT QMSDD, DHA-MUA-FBKT QMSDD in Section IV-D and the DHA-aided QWSA QMSDD in Section IV-E.

In Fig. 6 we showed that the DHA QMSDD offers an equivalent performance to the ML MSDD, while requiring fewer CFEs per bit. The ES-DHA QMSDD provides a tunable performance based on the affordable complexity budget, as demonstrated in Fig. 8. We showed in Fig. 9 and Fig. 10 that the DHA-MAA and the DHA-MAA-NE QMSDDs are unsuitable for integration with iterative receivers, but they provide a near-optimal performance at a low complexity during the first MSDD-DEC iteration. The family of DHA-MUA QMSDDs may be used in a receiver, as presented in Fig. 12, where iterations are carried out between the MSDD and the DEC, hence achieving a BER performance, which is less than 1 dB away from that of the optimal MAP MSDD's performance, as depicted in Fig. 11.

Moreover, in Section V we proposed a methodology for deterministically initializing the DHA searches of the QMSDDs, by employing the CDD, while waiting for the signals that participate in a detection window to arrive and hence acquiring an early estimate of the optimal symbol. In the scenarios, when the CDD estimate turns out to be the same as the MSDD's estimate, or close to it in terms of its Hamming distance, the complexity reduction achieved is higher. As seen in Fig. 17 and Table 7, the impact of the CDD initialization on the complexity is more apparent in the HIHO DHA and ES-DHA QMSDDs, where the objective is to simply find the globally optimal multi-level symbol. In the case of the SISO DHA-based QMSDDs, the CDD-initialized QMSDDs require approximately the same complexity as the randomly-initialized QMSDDs, due to their more complex methodology. For this reason, we proposed the *iteration memory* concept of Section V-B for the SISO QMSDDs, where the globally optimal symbol found during a single MSDD-DEC iteration is used for initializing the DHA

searches of the next MSDD-DEC iteration, hence further reducing the complexity.

Furthermore, motivated by our quest for low-complexity QMSDDs, we proposed the reuse of the symbol set created by the SISO DHA-based QMSDDs during a single QMSDD-DEC iteration in $(IpS - 1)$ of the subsequent QMSDD-DEC iterations, hence reducing the complexity, since the QMSDD was not employed in those iterations. We found that the system performance associated with $IpS > 1$ was close to that of the scenario, where the QMSDD is employed during every QMSDD-DEC iteration, albeit the corresponding complexity was lower for $IpS > 1$.

Finally, in Fig. 22, Fig. 23, Fig. 24 and Fig. 25 we investigated the effect of the detection window length N_w, of the subcarrier-hopping period T_h and of the interleaver length on the system's performance. The parameters having the highest impact were the interleaver length and the detection window length N_w, with the subcarrier-hopping period T_h having a much lower effect on the system's BER. The proposed QMSDDs will result in a higher performance gain with respect to that of the CDD in systems with excessively high Doppler frequency, where the CDD experiences an BER floor.

Apart from the challenges of near-optimal non-coherent detection at a low complexity, there is a number of open problems in wireless systems that may be efficiently tackled by quantum computing and quantum search algorithms. It may be beneficial to create a joint quantum MUD and decoder, by incorporating the forward error correction metric into the multiple-stream detection metric. Moreover, quantum-assisted turbo synchronization and channel estimation may prove less complex than the existing algorithms, while the Minimum BER (MBER) criterion may be adopted for performing quantum-assisted turbo synchronization, channel estimation and detection [67], [68]. A study, which benchmarks the quantum-assisted solutions against the best known bio-inspired algorithms [3], [69]–[72] may prove beneficial. Quantum search algorithms may also be used in the context of network coding [73], [74]. Furthermore, the quantum search algorithms employed in this treatise are assumed to operate in an error-free environment. In practice, based on the imperfections of the materials that will be used to create the quantum gates, the qubits may have a non-zero probability of changing their states [57], [58], leading to undesirable search outcomes. Modelling the effects of specific materials as a quantum channel, we may be able to use quantum error correction codes [75], [76] for stabilizing the quantum states in the quantum circuits.

REFERENCES

[1] M. Dong and L. Tong, "Optimal design and placement of pilot symbols for channel estimation," *IEEE Trans. Signal Process.*, vol. 50, no. 12, pp. 3055–3069, Dec. 2002.

[2] A. Vosoughi and A. Scaglione, "Everything you always wanted to know about training: Guidelines derived using the affine precoding framework and the CRB," *IEEE Trans. Signal Process.*, vol. 54, no. 3, pp. 940–954, Mar. 2006.

[3] L. Hanzo, Y. Akhtman, M. Jiang, and L. Wang, *MIMO-OFDM for LTE, WIFI and WIMAX: Coherent Versus Non-Coherent and Cooperative Turbo-Transceivers*. New York, NY, USA: Wiley, 2010.

[4] L. Wang and L. Hanzo, "Dispensing with channel estimation: Differentially modulated cooperative wireless communications," *IEEE Commun. Surveys Tuts.*, vol. 14, no. 13, pp. 836–857, Mar. 2012.

[5] L. Wang, L. Li, C. Xu, D. Liang, S. X. Ng, and L. Hanzo, "Multiple-symbol joint signal processing for differentially encoded single- and multi-carrier communications: Principles, designs and applications," *IEEE Commun. Surveys Tuts.*, vol. 16, no. 2, pp. 689–712, Feb. 2014.

[6] V. Buchoux, O. Cappe, E. Moulines, and A. Gorokhov, "On the performance of semi-blind subspace-based channel estimation," *IEEE Trans. Signal Process.*, vol. 48, no. 6, pp. 1750–1759, Jun. 2000.

[7] E. de Carvalho and D. T. M. Slock, "Blind and semi-blind FIR multichannel estimation: (Global) identifiability conditions," *IEEE Trans. Signal Process.*, vol. 52, no. 4, pp. 1053–1064, Apr. 2004.

[8] L. Tong, R. Liu, V. C. Soon, and Y.-F. Huang, "Indeterminacy and identifiability of blind identification," *IEEE Trans. Circuits Syst.*, vol. 38, no. 5, pp. 499–509, May 1991.

[9] L. Tong and S. Perreau, "Multichannel blind identification: From subspace to maximum likelihood methods," *Proc. IEEE*, vol. 86, no. 10, pp. 1951–1968, Oct. 1998.

[10] M. C. Necker and G. L. Stuber, "Totally blind channel estimation for OFDM on fast varying mobile radio channels," *IEEE Trans. Wireless Commun.*, vol. 3, no. 5, pp. 1514–1525, Sep. 2004.

[11] G. Brassard, F. Dupuis, S. Gambs, and A. Tapp. (Jun. 2011). "An optimal quantum algorithm to approximate the mean and its application for approximating the median of a set of points over an arbitrary distance." [Online]. Available: http://arxiv.org/abs/1106.4267

[12] P. Botsinis, S. X. Ng, and L. Hanzo, "Fixed-complexity quantum-assisted multi-user detection for CDMA and SDMA," *IEEE Trans. Commun.*, vol. 62, no. 3, pp. 990–1000, Mar. 2014.

[13] P. Botsinis, D. Alanis, S. X. Ng, and L. Hanzo, "Low-complexity soft-output quantum-assisted multiuser detection for direct-sequence spreading and slow subcarrier-hopping aided SDMA-OFDM systems," *IEEE Access*, vol. 2, pp. 451–472, May 2014.

[14] P. Botsinis, S. X. Ng, and L. Hanzo, "Quantum search algorithms, quantum wireless, and a low-complexity maximum likelihood iterative quantum multi-user detector design," *IEEE Access*, vol. 1, pp. 94–122, May 2013.

[15] A. Malossini, E. Blanzieri, and T. Calarco, "Quantum genetic optimization," *IEEE Trans. Evol. Comput.*, vol. 12, no. 2, pp. 231–241, Apr. 2008.

[16] S. Imre, "Quantum existence testing and its application for finding extreme values in unsorted databases," *IEEE Trans. Comput.*, vol. 56, no. 5, pp. 706–710, May 2007.

[17] S. Imre and F. Balázs, "Non-coherent multi-user detection based on quantum search," in *Proc. IEEE Int. Conf. Commun. (ICC)*, vol. 1. May 2002, pp. 283–287.

[18] S. Imre and F. Balázs, "Performance evaluation of quantum based multiuser detector," in *Proc. IEEE 7th Int. Symp. Spread Spectr. Techn. Appl.*, vol. 3. Sep. 2002, pp. 722–725.

[19] T. Hogg, "Quantum search heuristics," *Phys. Rev. A*, vol. 61, no. 5, p. 052311, Apr. 2000.

[20] T. Hogg and D. Portnov, "Quantum optimization," *Inf. Sci.*, vol. 128, nos. 3–4, pp. 181–197, 2000.

[21] C. Durr and P. Høyer. (Jul. 1996). "A quantum algorithm for finding the minimum." [Online]. Available: http://arxiv.org/abs/quant-ph/9607014

[22] D. Ventura and T. Martinez. (Jul. 1998). "Quantum associative memory." [Online]. Available: http://arxiv.org/abs/quant-ph/9807053

[23] G. Brassard, P. Høyer, and A. Tapp. (May 1998). "Quantum counting." [Online]. Available: http://arxiv.org/abs/quant-ph/9805082

[24] M. Boyer, G. Brassard, P. Høyer, and A. Tapp, "Tight bounds on quantum searching," *Fortschritte Phys.*, vol. 46, nos. 4–5, pp. 493–505, 1998.

[25] P. W. Shor, "Algorithms for quantum computation: Discrete logarithms and factoring," in *Proc. 35th Annu. Symp. Found. Comput. Sci.*, Nov. 1994, pp. 124–134.

[26] D. Deutsch and R. Jozsa, "Rapid solution of problems by quantum computation," *Proc., Math. Phys. Sci.*, vol. 439, no. 1907, pp. 553–558, Dec. 1992.

[27] D. Deutsch, "Quantum theory, the Church–Turing principle and the universal quantum computer," *Proc. Roy. Soc. London A, Math. Phys. Sci.*, vol. 400, no. 1818, pp. 97–117, 1985.

[28] R. P. Feynman, "Simulating physics with computers," *Int. J. Theoretical Phys.*, vol. 21, nos. 6–7, pp. 467–488, Jun. 1982.

[29] G. Brassard, P. Høyer, M. Mosca, and A. Tapp. (May 2000). "Quantum amplitude amplification and estimation." [Online]. Available: http://arxiv.org/abs/quant-ph/0005055

[30] J. C. Garcia-Escartin and P. Chamorro-Posada, "Quantum spread spectrum multiple access," *IEEE J. Sel. Topics Quantum Electron.*, vol. 21, no. 3, May/Jun. 2015, Art. ID 6400107.

[31] L. K. Grover, "A fast quantum mechanical algorithm for database search," in *Proc. 28th Annu. ACM Symp. Theory Comput.*, May 1996, pp. 212–219.

[32] L. K. Grover, "Quantum mechanics helps in searching for a needle in a haystack," *Phys. Rev. Lett.*, vol. 79, no. 2, pp. 325–328, Jul. 1997.

[33] J. K. Cavers, "An analysis of pilot symbol assisted modulation for Rayleigh fading channels [mobile radio]," *IEEE Trans. Veh. Technol.*, vol. 40, no. 4, pp. 686–693, Nov. 1991.

[34] T. S. Rappaport *et al.*, "Millimeter wave mobile communications for 5G cellular: It will work!" *IEEE Access*, vol. 1, pp. 335–349, May 2013.

[35] S. Sugiura, S. Chen, and L. Hanzo, "MIMO-aided near-capacity turbo transceivers: Taxonomy and performance versus complexity," *IEEE Commun. Surveys Tuts.*, vol. 14, no. 2, pp. 421–442, May 2012.

[36] L. Hanzo, H. Haas, S. Imre, D. O'Brien, M. Rupp, and L. Gyongyosi, "Wireless myths, realities, and futures: From 3G/4G to optical and quantum wireless," *Proc. IEEE*, vol. 100, no. Special Centennial Issue, pp. 1853–1888, May 2012.

[37] J. Hoydis, S. ten Brink, and M. Debbah, "Massive MIMO in the UL/DL of cellular networks: How many antennas do we need?" *IEEE J. Sel. Areas Commun.*, vol. 31, no. 2, pp. 160–171, Feb. 2013.

[38] D. Divsalar and M. K. Simon, "Multiple-symbol differential detection of MPSK," *IEEE Trans. Commun.*, vol. 38, no. 3, pp. 300–308, Mar. 1990.

[39] F. Adachi and M. Sawahashi, "Decision feedback multiple-symbol differential detection for M-ary DPSK," *Electron. Lett.*, vol. 29, no. 15, pp. 1385–1387, Jul. 1993.

[40] K. Mackenthun, Jr., "A fast algorithm for multiple-symbol differential detection of MPSK," *IEEE Trans. Commun.*, vol. 42, no. 234, pp. 1471–1474, Feb./Apr. 1994.

[41] M. Peleg and S. Shamai, "Iterative decoding of coded and interleaved noncoherent multiple symbol detected DPSK," *Electron. Lett.*, vol. 33, no. 12, pp. 1018–1020, Jun. 1997.

[42] L. Hanzo, S. X. Ng, W. Webb, and T. Keller, *Quadrature Amplitude Modulation: From Basics to Adaptive Trellis-Coded, Turbo-Equalised and Space-Time Coded OFDM, CDMA and MC-CDMA Systems*. New York, NY, USA: Wiley, Sep. 2004.

[43] P. Yang, Y. Xiao, B. Zhang, S. Li, M. El-Hajjar, and L. Hanzo, "Star-QAM signaling constellations for spatial modulation," *IEEE Trans. Veh. Technol.*, vol. 63, no. 8, pp. 3741–3749, Oct. 2014.

[44] S. Sugiura, C. Xu, S. X. Ng, and L. Hanzo, "Reduced-complexity coherent versus non-coherent QAM-aided space-time shift keying," *IEEE Trans. Commun.*, vol. 59, no. 11, pp. 3090–3101, Nov. 2011.

[45] D. Divsalar and M. K. Simon, "Maximum-likelihood differential detection of uncoded and trellis coded amplitude phase modulation over AWGN and fading channels-metrics and performance," *IEEE Trans. Commun.*, vol. 42, no. 1, pp. 76–89, Jan. 1994.

[46] P. Ho and D. Fung, "Error performance of multiple-symbol differential detection of PSK signals transmitted over correlated Rayleigh fading channels," *IEEE Trans. Commun.*, vol. 40, no. 10, pp. 1566–1569, Oct. 1992.

[47] R. Schober, W. H. Gerstacker, and J. B. Huber, "Decision-feedback differential detection of MDPSK for flat Rayleigh fading channels," *IEEE Trans. Commun.*, vol. 47, no. 7, pp. 1025–1035, Jul. 1999.

[48] H. Leib, "Data-aided noncoherent demodulation of DPSK," *IEEE Trans. Commun.*, vol. 43, nos. 2–4, pp. 722–725, Feb./Apr. 1995.

[49] R. Schober and W. H. Gerstacker, "Decision-feedback differential detection based on linear prediction for MDPSK signals transmitted over Ricean fading channels," *IEEE J. Sel. Areas Commun.*, vol. 18, no. 3, pp. 391–402, Mar. 2000.

[50] L. Lampe, R. Schober, V. Pauli, and C. Windpassinger, "Multiple-symbol differential sphere decoding," *IEEE Trans. Commun.*, vol. 53, no. 12, pp. 1981–1985, Dec. 2005.

[51] C. Xu, S. Sugiura, S. X. Ng, and L. Hanzo, "Reduced-complexity noncoherently detected differential space-time shift keying," *IEEE Signal Process. Lett.*, vol. 18, no. 3, pp. 153–156, Mar. 2011.

[52] C. Xu, L. Wang, S. X. Ng, and L. Hanzo, "Multiple-symbol differential sphere detection aided differential space-time block codes using QAM constellations," *IEEE Signal Process. Lett.*, vol. 18, no. 9, pp. 497–500, Sep. 2011.

[53] L. H.-J. Lampe and R. Schober, "Low-complexity iterative demodulation for noncoherent coded transmission over Ricean-fading channels," *IEEE Trans. Veh. Technol.*, vol. 50, no. 6, pp. 1481–1496, Nov. 2001.

[54] L. H.-J. Lampe and R. Schober, "Iterative decision-feedback differential demodulation of bit-interleaved coded MDPSK for flat Rayleigh fading channels," *IEEE Trans. Commun.*, vol. 49, no. 7, pp. 1176–1184, Jul. 2001.

[55] P. Hoeher and J. Lodge, "'Turbo DPSK': Iterative differential PSK demodulation and channel decoding," *IEEE Trans. Commun.*, vol. 47, no. 6, pp. 837–843, Jun. 1999.

[56] V. Pauli, L. Lampe, and R. Schober, "'Turbo DPSK' using soft multiple-symbol differential sphere decoding," *IEEE Trans. Inf. Theory*, vol. 52, no. 4, pp. 1385–1398, Apr. 2006.

[57] M. A. Nielsen and I. L. Chuang, *Quantum Computation and Quantum Information*. Cambridge, U.K.: Cambridge Univ. Press, 2000.

[58] S. Imre and F. Balázs, *Quantum Computing and Communications: An Engineering Approach*. New York, NY, USA: Wiley, 2005.

[59] S. Imre and L. Gyongyosi, *Advanced Quantum Communications: An Engineering Approach*. New York, NY, USA: Wiley, 2013.

[60] P. Botsinis, S. X. Ng, and L. Hanzo, "Low-complexity iterative quantum multi-user detection in SDMA systems," in *Proc. IEEE Int. Conf. Commun. (ICC)*, Jun. 2014, pp. 5592–5597.

[61] J. G. Proakis, *Digital Communications*, 4th ed. New York, NY, USA: McGraw-Hill, 2001.

[62] L. Hanzo, M. Münster, B. Choi, and T. Keller, *OFDM and MC-CDMA for Broadband Multi-User Communications, WLANs and Broadcasting*. New York, NY, USA: Wiley, 2003.

[63] D. Alanis, P. Botsinis, S. X. Ng, and L. Hanzo, "Quantum-assisted routing optimization for self-organizing networks," *IEEE Access*, vol. 2, pp. 614–632, Jun. 2014.

[64] S. Sesia, I. Toufik, and M. Baker, *LTE, The UMTS Long Term Evolution: From Theory to Practice*. New York, NY, USA: Wiley, 2009.

[65] Y.-M. Chen, Y.-L. Ueng, and H.-J. Shiau, "An EXIT-based design method for LDPC-coded schemes without Gaussian assumptions," *IEEE Commun. Lett.*, vol. 17, pp. 1648–1651, Aug. 2013.

[66] J. Hagenauer, "The EXIT chart—Introduction to extrinsic information transfer," in *Proc. 12th Eur. Signal Process. Conf. (EUSIPCO)*, 2004, pp. 1541–1548.

[67] A. K. Dutta, K. V. S. Hari, and L. Hanzo, "Channel estimation relying on the minimum bit-errorratio criterion for BPSK and QPSK signals," *IET Commun.*, vol. 8, no. 1, pp. 69–76, Jan. 2014.

[68] A. Dutta, K. Hari, and L. Hanzo, "Minimum-error-probability CFO estimation for muti-user MIMO OFDM systems," *IEEE Trans. Veh. Technol.*, Aug. 2014.

[69] S. X. Ng, K. Yen, and L. Hanzo, "M-ary coded modulation assisted genetic algorithm based multiuser detection for CDMA systems," in *Proc. IEEE Wireless Commun. Netw. Conf.*, vol. 2. Mar. 2003, pp. 779–783.

[70] L. Hanzo, L.-L. Yang, E.-L. Kuan, and K. Yen, *Single and Multi-Carrier DS-CDMA: Multi-User Detection, Space-Time Spreading, Synchronisation, Networking and Standards*. New York, NY, USA: Wiley, 2003.

[71] M. Jiang, S. X. Ng, and L. Hanzo, "Hybrid iterative multiuser detection for channel coded space division multiple access OFDM systems," *IEEE Trans. Veh. Technol.*, vol. 55, no. 1, pp. 115–127, Jan. 2006.

[72] M. Jiang and L. Hanzo, "Multiuser MIMO-OFDM for next-generation wireless systems," *Proc. IEEE*, vol. 95, no. 7, pp. 1430–1469, Jul. 2007.

[73] W. Chen, L. Hanzo, and Z. Cao, "Network coded modulation for two-way relaying," in *Proc. IEEE Wireless Commun. Netw. Conf.*, Mar. 2011, pp. 1765–1770.

[74] W. Chen, Z. Cao, and L. Hanzo, "Maximum Euclidean distance network coded modulation for asymmetric decode-and-forward two-way relaying," *IET Commun.*, vol. 7, no. 1, pp. 988–998, Jul. 2013.

[75] Z. Babar, S. X. Ng, and L. Hanzo, "Near-capacity code design for entanglement-assisted classical communication over quantum depolarizing channels," *IEEE Trans. Commun.*, vol. 61, no. 12, pp. 4801–4807, Dec. 2013.

[76] Z. Babar, S. X. Ng, and L. Hanzo, "EXIT-chart-aided near-capacity quantum turbo code design," *IEEE Trans. Veh. Technol.*, vol. 64, no. 3, pp. 866–875, Mar. 2015.

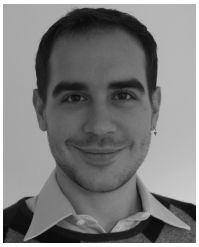

PANAGIOTIS BOTSINIS (S'12) received the Diploma degree from the School of Electrical and Computer Engineering, National Technical University of Athens, Greece, in 2010, and the M.Sc. (Hons.) degree in wireless communications from the University of Southampton, U.K., in 2011. He is currently pursuing the Ph.D. degree with the Southampton Wireless, School of Electronics and Computer Science, University of Southampton. Since 2010, he has been a member of the Technical Chamber of Greece.

His research interests include quantum-assisted communications, quantum computation, iterative detection, orthogonal frequency domain multiplexing, MIMO, multiple access systems, coded modulation, channel coding, cooperative communications, and combinatorial optimization.

DIMITRIOS ALANIS (S'13) received the M.Eng. degree in electrical and computer engineering from the Aristotle University of Thessaloniki, in 2011, and the M.Sc. degree in wireless communications from the University of Southampton, in 2012. He is currently pursuing the Ph.D. degree with the Southampton Wireless, School of Electronics and Computer Science, University of Southampton.

Dimitrios's research interests include quantum computation and quantum information theory, quantum search algorithms, cooperative communications, resource allocation for self-organizing networks, bioinspired optimization algorithms, and classical and quantum game theory.

ZUNAIRA BABAR received the B.Eng. degree in electrical engineering from the National University of Science and Technology, Islamabad, Pakistan, in 2008, and the M.Sc. (Hons.) degree in wireless communications from the University of Southampton, U.K., in 2011, where she is currently pursuing the Ph.D. degree with the Southampton Wireless, School of Electronics and Computer Science. Her research interests include quantum error correction codes, channel coding, coded modulation, iterative detection, and cooperative communications.

SOON XIN NG (S'99–M'03–SM'08) received the B.Eng. (Hons.) degree in electronics engineering and the Ph.D. degree in wireless communications from the University of Southampton, Southampton, U.K., in 1999 and 2002, respectively. From 2003 to 2006, he was a Post-Doctoral Research Fellow working on collaborative European research projects known as SCOUT, NEWCOM, and PHOENIX. Since 2006, he has been an Academic Staff Member with the School of Electronics and Computer Science, University of Southampton. He is involved in the OPTIMIX and CONCERTO European projects, and the IUATC and UC4G projects. He is currently an Associate Professor of Telecommunications with the University of Southampton.

He has authored over 180 papers and co-authored two John Wiley/IEEE Press books in his research field. His research interests include adaptive coded modulation, coded modulation, channel coding, space–time coding, joint source and channel coding, iterative detection, orthogonal frequency domain multiplexing, MIMO, cooperative communications, distributed coding, quantum error correction codes, and joint wireless-and-optical-fiber communications. He is a Chartered Engineer and a fellow of the Higher Education Academy in the U.K.

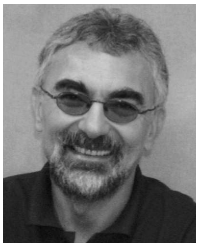

LAJOS HANZO (M'91–SM'92–F'04) received the degree in electronics, in 1976, the Ph.D. degree, in 1983, and the D.Sc. degree from the Technical University of Budapest, in 2009. During the 37 years of career in telecommunications, he has held various research and academic positions in Hungary, Germany, and U.K. Since 1986, he has been with the School of Electronics and Computer Science, University of Southampton, U.K., where he holds the Chair in telecommunications. He has successfully supervised over 80 Ph.D. students, has co-authored 20 John Wiley/IEEE Press books in mobile radio communications totaling in excess of 10 000 pages, and has authored over 1400 research entries at the IEEE Xplore. He has over 19 000 citations. He is a fellow of the Future Institute of Engineering and Technology, and the European Association for Signal Processing. He is directing the 100-strong academic research team, working on a range of research projects in the field of wireless multimedia communications sponsored by the industry, the U.K. Engineering and Physical Sciences Research Council, the European Research Council Advanced Fellow Grant, and the Royal Society's Wolfson Research Merit Award. His research is funded by the European Research Council's Senior Research Fellow Grant. He has acted as the Technical Program Committee and General Chair of the IEEE conferences, presented keynote lectures, and received a number of distinctions. He is an enthusiastic supporter of industrial and academic liaison, and offers a range of industrial courses. He is also a Governor of the IEEE Vehicular Technology Society. From 2008 to 2012, he was the Editor-in-Chief of the IEEE Press and a Chair Professor with Tsinghua University, Beijing.